On the influence of debris cover on glacier morphology: How high-relief structures evolve from smooth surfaces.

Nico Mölg[1], James Ferguson[1], Tobias Bolch[2], Andreas Vieli[1]

[1]Department of Geography, University of Zurich, 8057 Zurich, Switzerland
[2]School of Geography and Sustainable Development, University of St Andrews, St Andrews, KY16 9A, Scotland, UK

Abstract

Debris-covered glaciers receive increasing attention during this period of sustained negative mass balance and expanding debris cover. The debris cover induces various feedback mechanisms that shape the evolution of the glacier geometry, and also of its surface. Although the surface morphology of many debris-covered glaciers is markedly different from that of debris-free glaciers, only a few studies have combined different processes to investigate these characteristic glacier surfaces in order to improve our knowledge of glacier evolution on a wider spatial and temporal scale. Debris-covered glacier tongues can consist of parts with a smooth surface as well as surfaces of high local relief with abundant ice cliffs in the lower end. In this study we analysed the evolution of the surface features of Zmuttgletscher, a debris-covered glacier in Switzerland, over a period of 140 years using time series of historic maps, high resolution digital elevation models and glacier velocities, as well as data on debris cover extent and thickness. Our results revealed insights into the up-glacier expansion of the debris cover over time and the formation of medial moraines in the prolongation of the uppermost areas where debris emerged on the glacier surface. Moraine ridge prominence increased during periods of negative mass balance, and troughs developed in debris-free areas between ridges, persisting even after a continuous debris cover had developed. The changing surface morphology inhibits across-glacier meltwater flow, both supra- and subglacially. Accordingly, we found that large cryo-valleys with ice cliffs have formed down-glacier of the troughs where meltwater runoff accumulates. The meanders of these valleys have enlarged over time, especially by ice cliff backwasting at steep slopes, and most of the glacier width today is affected by such high-relief erosion features. We find that about 75% of all ice cliffs are located in this high-relief zone. The volume lost at these erosion features has increased by a factor of five since the 1980s, but is still negligible in comparison to the high glacier-wide thinning rates.

1. Introduction

Tongues of temperate debris-free or little debris-covered valley glaciers are typically slightly convex with a smooth surface. In settings of high-relief topography, glaciers often develop a patchy or even continuous cover of supraglacial debris on their tongues, which increases in thickness towards the

terminus due to ice emergence, ablation, compressive flow, and the fact that low flow velocities impede the removal of the debris from the glacier system (e.g. Nakawo et al. 1986, Benn et al. 2012, Anderson and Anderson 2018). On these tongues a succession of more or less distinct zones with different surface morphology can develop (Iwata et al. 1980). Down-glacier of the bare ice zone, a partly debris-covered zone begins. Typically, the englacially transported debris emerges on the surface as elongated bands or transverse septa (e.g. Boulton 1978, Gomez and Small 1985, Vere and Benn 1989, Appleby et al. 2010, Kirkbride and Deline 2013, Jennings et al. 2014). Because thick supraglacial debris insulates the underlying ice, a patchy or heterogeneous debris cover leads to locally different ablation rates and even topographic inversion (Østrem 1959, Nicholson and Benn 2006, Mihalcea et al. 2008, Thompson et al. 2016, Nicholson et al. 2018). As a consequence of this differential ablation, elevated along-flow structures appear, and medial moraines form beneath the longitudinal debris bands at the glacier surface. Previous studies observed an increase in height of these medial moraines down-glacier, followed by a decrease again towards the terminus due to debris redistribution and ice deformation (Loomis 1970, Small and Clark 1974, Eyles and Rogerson 1978, Bozhinskiy et al. 1986). Down-glacier of this transition zone, sustained debris surfacing forms a continuous debris cover stretching over much of the tongue's width. In this zone, the debris often appears as a thin, homogeneous layer on a relatively smooth glacier surface, which is often characterised by along-flow moraine ridges. Further down-glacier, especially during periods of negative mass balance, the extent and thickness of this debris cover have been observed to increase (e.g. Nakawo et al. 1986, Benn et al. 2001, Kirkbride and Deline 2013, Mölg et al. 2019). On heavily debris-covered glaciers, thicker debris towards the terminus can lead to a reversal of the mass balance gradient and typically, long, gently-sloping, slow-flowing tongues develop, which can significantly delay glacial responses to climatic forcing (e.g. Kirkbride 2002, Benn et al. 2012, Bolch et al. 2012).

In these parts of the glacier tongue often a zone of high local relief is observed, in which typical surface features such as ice cliffs and ponds are embedded. This high-relief area exhibits local elevation differences of up to several tens of metres on short distances and is formed by valleys and depressions that seem to be mainly shaped by meltwater erosion and ice-cliff backwasting (Iwata et al. 1980). Ice cliffs and ponds seem to contribute disproportionately to the glacier-wide ablation (e.g. Sakai et al. 2002, Juen et al. 2014, Brun et al. 2016, Ragettli et al. 2016). Consequently, these features have been attracting a lot of attention in the recent literature, and major advances have been achieved regarding both their automatic detection (e.g. Kraaijenbrink et al. 2016, Herreid and Pellicciotti 2018) and their ablation rates and energy balance (Sakai et al. 2002, Röhl 2008, Han et al. 2010, Buri et al. 2016, Buri and Pellicciotti 2018). However, only a few studies have estimated the influence of ice cliffs and meltwater erosion features (hereafter called erosion features) over decadal periods (e.g. Ragettli et al.

2016, Mölg et al. 2019). Despite the proposition of several mechanisms for the formation of ice cliffs, namely subsidence of the surface, calving, and sliding off of debris from steep surfaces (Kirkbride 1993, Benn et al. 2001, Reid and Brock 2014), the process understanding regarding their genesis has not yet been fully clarified, and current explanations of the formation of ice-cliff prone zones remain vague in terms of the wider glacio-geomorphogenetic context.

The long-term influence of debris cover on mass balance gradient, glacier geometry and flow dynamics is now widely recognised, but the evolution of debris-related glacier surface morphology and the described zones have received little attention, although they are found on many debris-covered glaciers worldwide. Observing their evolution over longer time scales has the potential to bring new insights into the formation and relevance of these zones and the mutual influences of their succession both spatially, along the glacier tongue, as well as temporally. Mainly due to data constraints, the different morphological elements have rarely been investigated for time scales long enough to allow for their formation to be ascribed to specific processes.

For Zmuttgletscher, a debris-covered glacier in the Swiss Alps, a set of eleven digital elevation models (DEMs) from 1879 – soon after the end of the Little Ice Age (LIA) – until 2018 is available together with orthophotos of high resolution since 1946 (cf. Mölg and Bolch 2017, Mölg et al. 2019), along with in-situ measurements of debris and ice thickness. This long-term dataset allows for a thorough investigation of the different morphological zones, their main elements, and their evolution over several decades. The objectives of this study are to

- understand the evolution and transition of the zones of low relief and high relief since 1879,
- explain the formation of the observed ridges and troughs in the low-relief zone,
- explain the formation of the erosion features including ice cliffs and debris cones in the high-relief zone,
- and analyse the changes of the erosion features in area and volume over time to quantify their contribution to glacier-wide thinning.

2. Study site

Zmuttgletscher (45°59’N, 7°37’E) is located in the Western Alps of Switzerland and has a surface area of ~16 km² and a length of ~7 km (year 2019). The glacier consists of a system of linked tributaries: Schönbielgletscher (SBG) and branch one of Stockjigletscher (STG1) from the North, and Tiefmattengletscher (TMG) and branch two of Stockjigletscher (STG2) from the South (Figure 1). The supraglacial debris cover extent increased from ~13% in 1859 to ~32% 2017 (Mölg et al. 2019), whereas changes in glacier area and length since the mid-20th century have been comparably small. Although the debris cover is extensive on Tiefmattengletscher and Schönbielgletscher,

Stockjigletscher is almost debris-free and accordingly the two branches of this glacier showed the strongest changes. The glacier terminus was stable between 1977 and 2001, with even a slight advance (see terminal moraine in Figure 1). Today, the tongue is nourished solely from Tiefmattengletscher and its headwalls. Old maps and the orthophoto from 1946 confirm the contribution of Schönbielgletscher and Stockjigletscher branch one until approximately the mid-20th century (supplementary Figure 1). Branch two of Stockjigletscher detached from the main glacier tongue around 2010.

Large parts of Zmuttgletscher have become debris-covered only during recent decades (Mölg et al. 2019). There were no previous studies on the topic of debris cover before the mentioned reference study. A substantial share of the debris-covered area is of rather low relief, where pronounced topography and large ice cliffs are missing. Instead, the low-relief zone is characterised by a relatively smooth debris-covered surface with along-flow ridges and troughs of varying height. The low-lying, high-relief zone of Zmuttgletscher is characterised by distinct erosion features, hollows, ice cliffs, debris cones, and a generally chaotic topography.

Air temperatures have risen since the end of the LIA in the 1850s, which has led to an almost continuously negative mass balance since 1879 (Mölg et al. 2019). In the 1920s and similarly in the 1970s climate conditions were more favourable for the glacier and hence mass balance was less negative or even slightly positive, thus leading to increased flow velocities at the glacier tongue. Velocities strongly declined again from the 1990s onwards combined with an even more negative mass balance and stronger air temperature increase. Since ~2005, the lowest ~1.5 km of the tongue is stagnant. The surface slope of the tongue increased from 9° to 11° from 1946-2018. The snow line evolution of monitored glaciers in the region documented a rise of the climatic Equilibrium Line Altitude (ELA) of ~300 m since the 1960s/1970s (Glacier du Giétro, Griesgletscher, Findelgletscher, Silvretta, Allalingletscher, Ghiacciao del Basòdino; GLAMOS 2018, World Glacier Monitoring Service 2018), suggesting an average ELA of ~3200 m (similar to nearby Findelgletscher) for the period of 2012-2018. This means that up until then, the ELA has risen above the foot of most of the headwalls that contribute mass (ice and snow avalanches including debris) to the main glacier tongue.

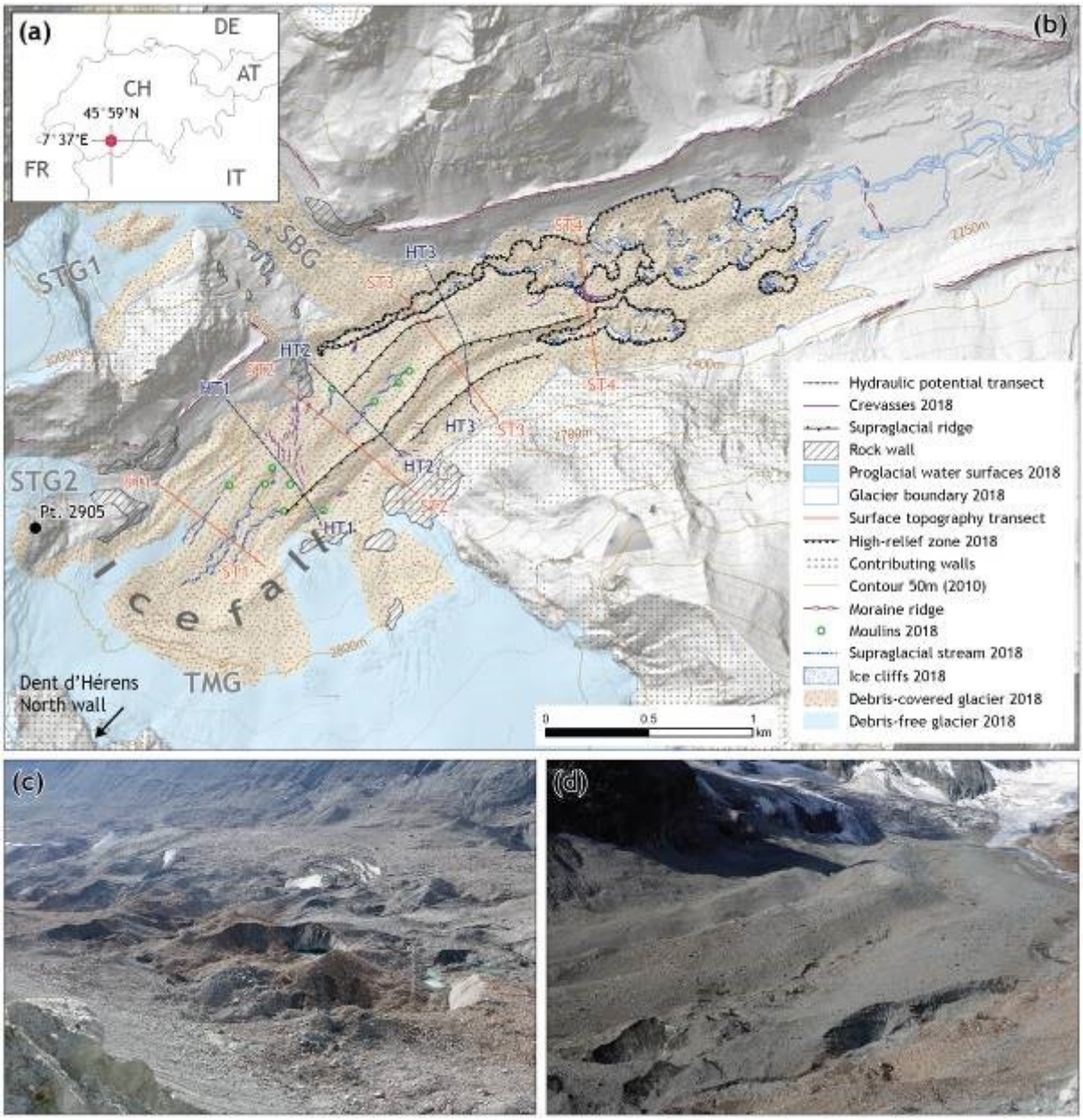

Figure 1: (a): Location of the study site. (b): Zmuttgletscher's ablation area in 2018 with morphologically mapped features on the glacier surface (see legend). Surface elevation transects (ST1-4) are shown in red and the hydropotential and bed transects (HT1-3) in dashed blue. SBG = Schönbielgletscher, STG = Stockjigletscher, TMG = Tiefmattengletscher. Geomorphologic symbols from Otto and Dikau (2004). (c): Lower part of the high-relief area and (d) the low-relief area on Zmuttgletscher seen from the left lateral moraine.

3. Data and methods

3.1. Overview and general approach

Our main data sources are historical maps, airplaine-based and UAV-based aerial photographs, from which we derived DEMs and orthophotos (Table 1). We also included field data consisting of debris thickness measurements, profiles of ice thickness (glacier bed), and surface observations on moulins, crevasses, and erosion features.

*Table 1: Input data overview. Abbreviations: OP = orthophoto, obl. aer. = oblique aerial, man. excav. = manual excavation, thickn. = thickness, elev. = elevation. Products denoted with * are taken as a final product from Swisstopo (2010). Ice thickness data were acquired by ETH Zurich and processed according to Langhammer et al. (2019). All other data were produced by Mölg and Bolch (2017) and Mölg et al. (2019).*

Date	Product	Source	Used for						Vertical uncer-tainty (m)	Spatial resol. (m), DTM / OP
			Elev. change	Debris cover	Cryo-valleys	Melt-water streams	Hydraul. potential	Ice cliffs		
1859	map	*Dufour map		x						
1879	DTM, map	*Siegfried map	x	x					~7	Hand-drawn (12m)
1930	Photo*	*Obl. aer. photo*	Photo used for surface features interpretation.							-
1946	DTM, OP	Aerial Stereo	x	x					5	8 / 0.5
1961	DTM, OP	Aerial Stereo	x	x					1	2 / 0.5
1977	DTM, OP	Aerial Stereo	x	x	x	x		x	1	4 / 0.4
1983	DTM, OP	Aerial Stereo	x		x			x	1.42	2 / 0.15
1988	DTM, OP	Aerial Stereo	x	x	x			x	1.19	5 / 0.35
1995	DTM, OP	Aerial Stereo	x		x			x	0.77	1 / 0.15
1999	OP*	Aerial Stereo*			x				-	- / 0.25
2001	DTM, OP	Aerial Stereo	x	x	x			x	1.39	1 / 0.35
2005	DTM, OP	Aerial Stereo	x		x			x	0.88	2 / 0.5
2007	OP*	Aerial Stereo*						x		- / 0.25
2010	DTM, OP*	Aerial Stereo*	x	x	x			x	2	2 / 0.25
03/2012	Ice thickn.	Aerial Radar					x		±10m	Point data
03/2017	Ice thickn.	Aerial Radar					x		±10m	Point data
2018	DTM, OP	UAV	x	x	x	x		x	1.5	0.5 / 0.15
09/2017	Debris thickn.	Man. excav.		x					0.02	Point data
09/2018	Debris thickn.	Man. excav.		x					0.02	Point data

3.2. Input data

Most relevant data, such as glacier surface topography, orthophotos, debris cover, and bed elevation, was obtained in previous work (Mölg and Bolch 2017, Mölg et al. 2019, Langhammer et al. 2019) and shall therefore only briefly be described here.

Glacier surface elevation for the year 1879 was extracted from the contour lines of the Siegfriedkarte (Swisstopo 2018). For all dates from 1946 to 2005, DEMs were generated from multiple stereo-imagery using the structure-from-motion software packages by Agisoft (Agisoft LLC 2016) and

Pix4Dmapper (Pix4D 2016; Mölg and Bolch 2017), and georeferenced with ground control points from the Swissimage orthophoto 2010 (Swisstopo 2010). The resulting DEMs yield resolutions between one and eight metres with vertical uncertainties between 0.77 m and 5 m after co-registration (Table 1; cf. Mölg and Bolch 2017). The DEM from 2018 is based on UAV imagery from a SenseFly ebee classic (SenseFly SA) and was produced with Pix4Dmapper. Orthophotos were generated by rectification of the aerial images using the respective DEMs. For the years 1999, 2007 and 2010, orthophotos from Swisstopo were used as a final product (Swisstopo 2010). All orthophotos have resolutions of 0.15-0.5 m (Table 1).

We analysed the evolution of the glacier surface morphology since 1879 along four transects perpendicular to the glacier flow (surface transects ST1-4, Figure 1). Debris cover extent is based on historical maps and orthophotos and is available for twelve dates since 1859 (Table 1). Debris thickness was gathered in-situ by manual excavation in September 2017 in the form of four cross profiles on the main tongue of Tiefmattengletscher, with altogether 77 data points (cf. Mölg et al. 2019). Values below 20 cm consist in an average of three measurements ~1 m apart to account for small-scale heterogeneity. In most areas, the debris cover is sufficiently thick to reduce ablation compared to clean ice (Mölg et al. 2019).

Helicopter-based ground-penetrating radar (GPR) measurements from March 2012 and March 2017 yielded ice thickness and bed elevation data for several cross-profiles on the glacier tongue (HT1-3, Figure 1). The GPR consisted of four 25 MHz unshielded dipole antennas by Sensors & Software (2017), separated by 4 m and fixed at the helicopter with a 14 m long rope. The spacing of the data points is 1 m and an uncertainty of ±10 m is assumed (VAW ETHZ, personal communication). A detailed description of the system and the data processing can be found in Langhammer et al. (2019).

3.3. Mapping of supraglacial streams, high-relief areas and ice cliffs

We analysed the orthophotos and mapped all the visible surface streams to link the location of supraglacial streams with surface morphology as well as with the onset of the high-relief zone further down-glacier. Supraglacial surface streams are defined as seasonal meltwater streams that shallowly incise into the ice. The mapped streams either disappeared in moulins or could be directly linked to supraglacial valleys (which we termed ´cryo-valleys´) further downstream. Moulins were mapped for the year 2018, supported by field visits from the same year. Note that it is not possible to map the complete sample of streams, since they exist in all sizes, are intermittent also during summer, and partly run below the debris cover.

Erosion features were mapped for the dates 1977, 1983, 1988, 1995, 2005, 2010, and 2018 in order to analyse the formation and evolution processes and the location of high-relief surface morphology.

Further, the volumes of these erosion features and the abundance of ice cliffs were quantified over the course of several decades. The mapping was done manually using sharp breaks in the surface slope of the respective DEMs, supported by the hillshade and the orthophotos in places where the surface slope did not show clear breaks (Figure 2). The mapping was done in a conservative way, i.e. closer to the feature centre in case of unclear feature boundaries, with the effect that the mapped area is rather smaller than the area actually affected by the erosion features, thus avoiding overestimation of their relevance. Repeated mapping of the same area showed an uncertainty range of ~5% of the total area, similar to glacier boundary mapping in debris-covered areas (Paul et al. 2013, Mölg et al. 2018). The erosion volume for each date was assessed using the following procedure: in the first step, the mapped erosion area was removed from the DEM. Secondly, this void DEM was interpolated using inversed distance weighting (Shepard 1968), which resulted in an artificial surface covering the erosion features at the elevation of the adjacent, non-eroded glacier surface. Finally, the erosion volume was calculated from the difference between the original (eroded) and the void-filled (interpolated) DEM (Figure 2).

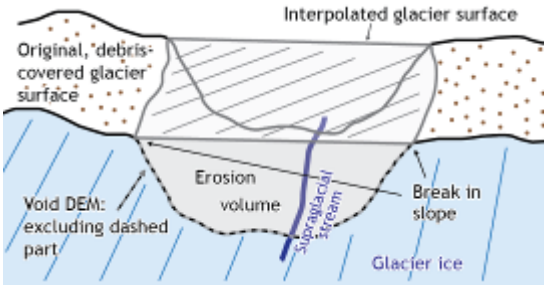

Figure 2: Illustration of the mapping of local erosion features. The volume below the grey plane was considered the erosion volume.

Ice cliffs were mapped (i) with an object-oriented image analysis approach using simple image segmentation from Trimble eCognition (eCognition Essentials 1.3 2016) and subsequent manual correction (c.f. Kraaijenbrink et al. 2016, Mölg et al. 2019), and (ii) by manual digitisation from the orthophoto for the year 2018.

3.4. Hydraulic potential

The flow of meltwater is important for the development of englacial voids and the corresponding surface expressions in the lowest part of glaciers (Benn et al. 2017). At the glacier surface, the flow path follows the steepest gradient. The englacial or subglacial flow is given by the gradient of the hydraulic potential ($\nabla\Phi$) which is influenced by the local surface and bed slope and by the englacial water head. As a first approximation, the water pressure is assumed to be at or close to the overburden pressure, which represents the case of a distributed basal drainage system. At the bed of the glacier, the hydraulic gradient $\nabla\Phi$ then becomes (Le Brocq et al. 2009):

$$\nabla\Phi = \rho_i * g * \nabla S + (\rho_w - \rho_i) * g * \nabla b \quad \text{Eq. 1}$$

where ρ_i and ρ_w are the densities of ice (917 kg m^{-3}) and water (1000 kg m^{-3}), respectively, g is the acceleration due to gravity, and ∇S and ∇b denote the gradients in elevation of the surface and the glacier bed, respectively. Note that when the appropriate constants are plugged into Eq. 1, the surface gradient becomes 10 times more important than the bed slope for the routing of the flow at the base of the glacier. The gradient of the hydraulic potential is only calculated in the direction of the three cross transects HT1-3 in the central part of the tongue, for which bed elevation data exist from GPR surveys (Figure 1).

3.5. Numerical model of ridge evolution

In order to further investigate some of the potential processes that drive the evolution of the observed medial moraine features in the low-relief zone, we use a simple and modified version of the medial moraine model by Anderson (2000) that captures the interplay between ice flow, debris melt-out, differential ablation due to variable debris thickness, and debris redistribution at the surface. In this model, we assume a steady state with regard to geometry, surface mass balance forcing and hence ice flow, and calculate the shape of cross-glacier surface transects at different locations along the direction of flow. Starting from conservation of the ice mass in steady state and using a representation of the effect of debris thickness on ablation rate that is consistent with the Østrem curve (e.g. inverse with debris thickness *D*, as in Anderson and Anderson 2016), we get:

$$u\frac{\partial H}{\partial x} = \frac{d_0 \dot{b}}{d_0 + D}$$

Here x is the along-flow direction, *H* is ice thickness, *D* is debris thickness, d_0 is a threshold debris thickness (taken here to be 5 cm) and $\dot{b}$ is surface mass balance that is linearly dependent on surface elevation (with a mass balance gradient of 0.007 yr^{-1}). The ice surface speed *u* is for our simple case of a constant bed gradient along the flow (and hence ice thickness) also a constant.

We couple this along-flow ice thickness evolution equation to an equation for debris thickness that includes down-glacier transport, redistribution across-glacier through a diffusion process, and melt-out of debris from the ice (following Anderson 2000):

$$u\frac{\partial D}{\partial x} + \beta\frac{\partial}{\partial y}\left(D\frac{\partial S}{\partial y}\right) = -\frac{c d_0 \dot{b}}{d_0 + D}$$

Here y is the across-flow direction, *S = H+D* is the debris-covered surface, *c* is the debris concentration within the ice and β is a diffusion constant that controls the strength of the diffusive process of debris redistribution across the glacier. Without any redistribution and ice deformation,

the moraine would grow almost linearly and indefinitely along the glacier. However, when debris redistribution and ice deformation dominate, moraines would not form since all surface features would quickly be smoothed out. Therefore, we used a medium-sized redistribution factor of 10, which captures a physically reasonable level of debris redistribution. Under slightly different conditions, Anderson (2000) uses a redistribution factor of β = 3 and our numerical experiments suggest that any value of a similar order of magnitude will yield similar qualitative results (see the supplementary material for more information). Further note that ice flow is parallel (no cross-glacier flow) and no ice deformation is considered in this model.

These coupled equations use a constant along-flow bed and surface slope and the approximate values of Zmuttgletscher glacier geometry, ice flow velocity (constant value of 30 m yr^{-1}), surface mass balance and debris thickness from Mölg et al. (2019). We used debris concentrations of 0.1% as a base level and 0.6% (left) and 0.7% (right) to produce the two medial moraines. A more detailed description of the model and the input data is provided in the supplementary material (text and Supplementary Table 1, Supplementary Figure 2, 3, 4, 5).

4. Results

The geomorphological map produced from orthophotos and field observations illustrates the general characteristics of the glacier surface (Figure 1, 10), the details for the transects ST1-4 are shown in Figure 3. Zmuttgletscher shows a clear along-flow succession of zones with different surface morphologies (Figure 1, 3, 10). The succession starts with the transition from bare ice to a discontinuous debris cover in the area below the icefall (see also Figure 1c) and is characterised by a relatively smooth surface. A number of supraglacial streams are found in this flat, central, debris-covered glacier part. A zone of continuous debris cover, without a clear boundary, is found immediately down-glacier. This zone still has a rather smooth glacier surface, but three elongated along-flow ridges of different heights have developed. Although these ridges show a substantial relief (between 10 and 40 m) in the across-flow direction, along the flow the slope of the ridges is almost constant. During this study, we will refer to these two parts as the low-relief zones. Their extent and position along the flow are not fixed but adjust over time in response to the evolution of the glacier and hence also to the climate forcing. Further down-glacier, they transition into a zone of high-relief topography, characterised by densely spaced topographic highs and lows, ice cliffs, a few supraglacial lakes, and signs of surface subsidence (eventually developing into circular cliffs).

In the following, we first present the evolution of the low-relief zones and the occurrence of surface streams. Thereafter, the transition of the surface morphology into the high-relief zone is described and interlinkages between surface morphology and meltwater are shown. We use the four surface transects ST1 to ST4 (Figure 1, 3) to present the evolution of surface morphology.

4.1. Evolution of the low-relief zone

An undulating but overall still smooth surface already existed in 1879 all along the glacier tongue (Figure 3), likely due to dynamic interaction between different tributaries rather than due to the effect of debris cover on the mainly debris-free tongue. The formation and evolution of medial moraine ridges is easy to follow both in time (1946-2017) and space (along the glacier tongue).

The area below the icefall is gently sloping and shows a smooth surface during most of the study period (ST1, Figure 3). Debris cover began to emerge in the mid-20th century (see lower part of the panels in Figure 3) and laterally expanded over time. In 2001, a smooth layer of debris covered most parts between ST1 and ST2. In the central glacier part in the uppermost transect (ST1) where debris first started to emerge, a small ridge (R2) started to form in the 1960s, disappeared again and then reappeared in 2010. This typical ablation-dominant medial moraine (cf. Eyles and Rogerson 1978) can be followed down-glacier at transects 2, 3 and 4 into the high-relief zone. At ST2, the central moraine ridge (R2) started to form after 1995 and constantly grew until 2010 (Figure 3, profile distance 500 m, panel ST2).

Further down-glacier, in the zone of continuous debris cover (e.g. ST3 and ST4), three distinct along-flow ridges developed during the study period (R1, R2, R3, from left to right, see Figure 3). At ST3, the ridges grew until 2010 with an interruption in the 1970s and 1980s. The glacier surface at ST2 and ST3 became steadily debris-covered during the 20th century, but the expansion was not consistent along the transect. A continuously narrowing band stayed debris-free until ~2005 and at this location a major trough developed between the two moraine ridges R2 and R3. Despite strong glacier thinning in the past two decades, the prominence of the central ridge R2 has persisted, while the ridges R1 and R3 have decreased in height.

The formation of ridges further down-glacier occurred earlier in time. At transect ST4, the same three ridges were already visible in 1946 (Figure 3). The peak of ridge formation was already reached in 1961 and afterwards their prominence decreased. At transect ST4 (profile distance 100-300 m in Figure 3) the glacier thinned considerably between 2010 and 2018 and the former ridge R1 disappeared, due to the enlargement of erosion features producing the high-relief area (see ST4 in Figure 1).

At all transects major troughs have developed in the debris-free sections (lower parts of panels in Figure 3, debris thickness indicated by red bars). The binary information on debris cover is supported by debris thickness information from 2017 and 2018. The thickest debris tends to occur on the ridges, but rather on the southern slopes than on the crests (Figure 3). At ST2-4, where most of the glacier surface is debris-covered today, the debris is thinner at the location of the troughs than on

the ridges to the left and right. The surface profiles also show that the location of the ridges and troughs has migrated slightly sideways over time, which is also visible in the debris cover panels, and we therefore attribute this to changes in glacier flow dynamics.

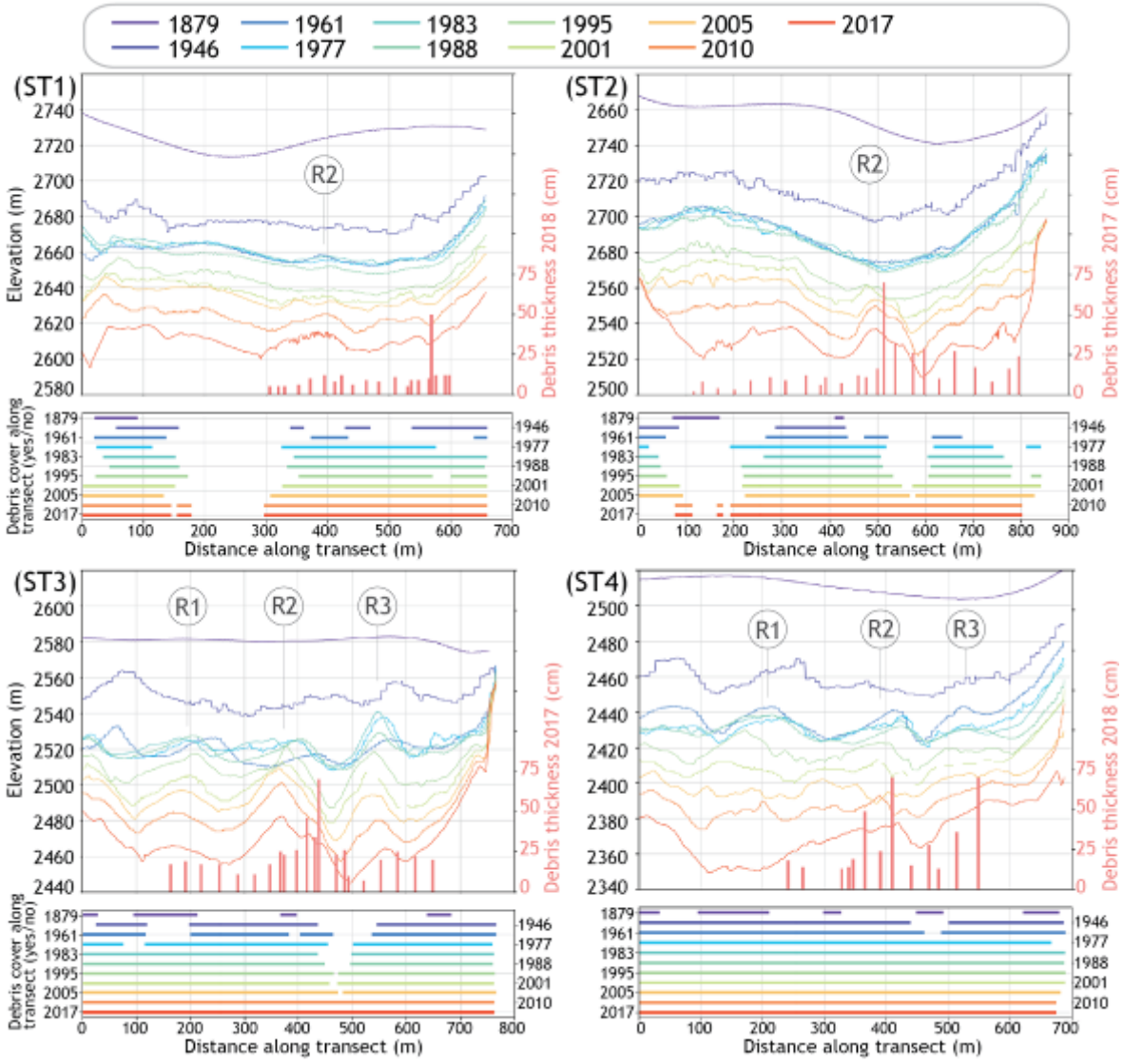

Figure 3: Evolution of ridges and troughs for transects ST1 through ST4 (indicated in Figure 1). The three main ridges are indicated: left ridge (R1), central ridge (R2) and right ridge. No data exist outside the outermost debris thickness measurements.

The prominence of the ridges was evaluated with their height, which is calculated as the vertical distance between the ridge's highest point and its neighbouring trough's lowest point, for each date since 1946 (Figure 4a). At ST2 the height of the central ridge (R2) was small (<10m) until 1995 (Figure 4b) but grew to heights of 20-30 m until 2010. Similar to ST2, ridge heights at transect ST3 grew strongly after 1961 and reached relatively stable heights between 25 and 45 m after 2000. At ST4 the ridges started to grow even before the 1960s after which they were roughly stable at 10-15 m, which is substantially lower than at the upper transects (Figure 4c). Also at ST4, in 2005 a major ice cliff

backwasted into the ridge, which caused the exceptionally low ridge height values and was readjusted through advected ice. Overall, the prominence of ridges has increased between 1946 and 2010, but has become stable and even decreased in the latest period between 2010 and 2018.

The succession of the different spatial zones as well as the relevant processes and the temporal development are summarised in detail in chapter 5 and in Figure 10.

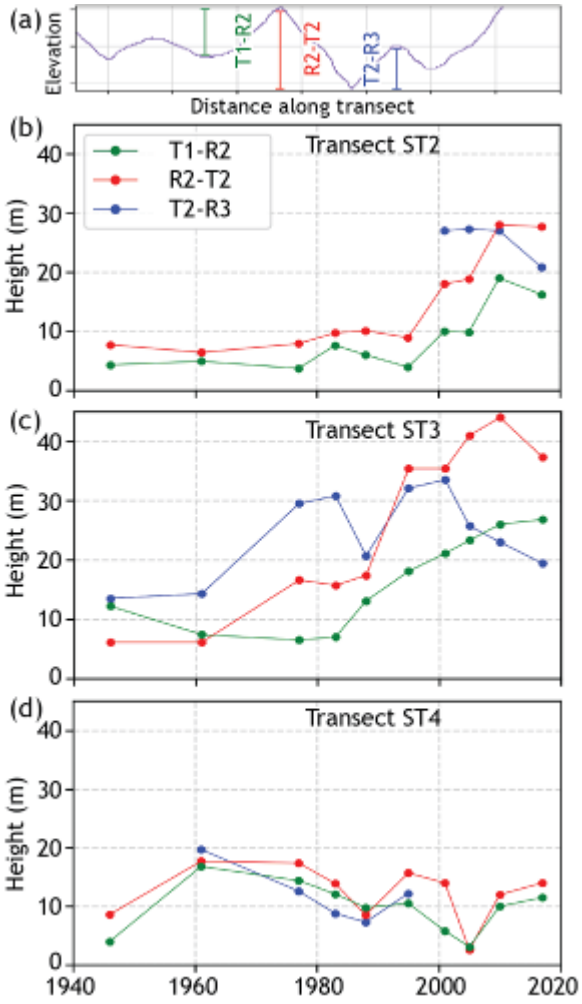

Figure 4: a): Indication of ridge and trough locations at the example of transect 3 in the year 2010. b-d): Evolution of the prominence of ridges R2 and R3 for transects ST2 (b), ST3 (c), and ST4 (d).

4.2. Modelled development of the low-relief area

The simple model of a hypothetical transect of varying debris concentration approximating the situation of Zmuttgletscher produced two medial moraines along the glacier tongue (Figure 5) due to contrasting ablation beneath the different debris thicknesses that developed. The modelling shows an almost linear increase in moraine height down the glacier that would continue unlimited for the case of no debris redistribution (dotted lines in Figure 5c). When including debris redistribution (as a diffusion process) the moraine heights stop growing at a certain distance and stagnate at heights comparable to the ones observed and then start to decrease slightly (Figure 5). This process is related

to a widening of the moraines and thinning-out of the debris on top due to the debris redistribution to their sides, combined with the continuous melt-out of debris in the troughs between the moraines. In a colder climate, the moraine emerges later (further down-glacier) and also the location at which the moraine height starts to stagnate and decrease is further down-glacier than for the warmer climate case. Here, the difference in climate is due to an ELA change of 100 m, which for the model geometry corresponds to a horizontal distance of 600 m. Interestingly, the maximum moraine heights are almost independent of climate. What is also different between cold and warm climate is that the moraine height starts to decrease again further up-glacier during the cold climate case. In general, the stagnation or even decrease in moraine heights mimics the observed evolution of the moraine height reasonably well.

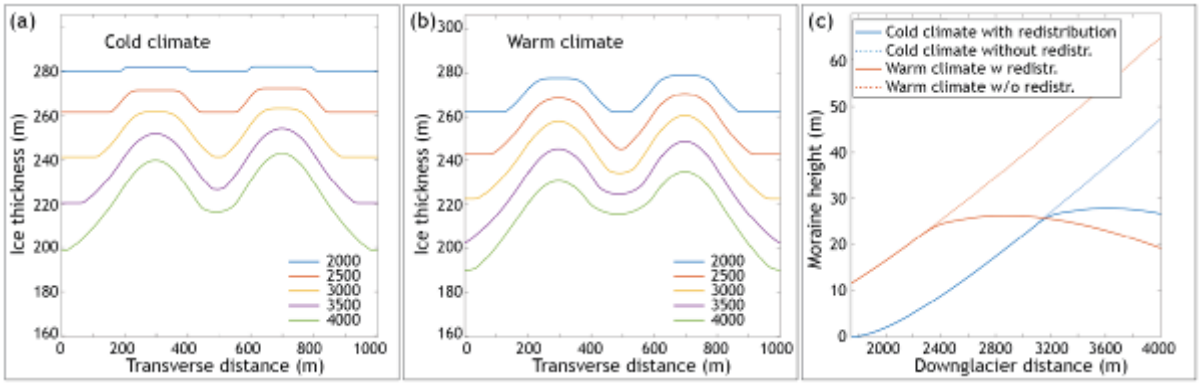

Figure 5: Modelled evolution of the ice surface (thickness) cross-transects for different positions along the glacier tongue (at the labelled distances in metres from the ELA) in (a) a cold climate and (b) a warm climate (with ΔELA=100 m). (c) shows the moraine height evolution with and without redistribution in a cold and warm climate.

4.3. Meltwater streams

Supraglacial meltwater streams are visible especially in the low-relief zone of the debris-covered area. One major stream cluster is located in the relatively flat area below the icefall, around transect ST1 (Figure 6). Large moulins drain the water of these streams into the glacier just above a small topographic step, where a number of transverse crevasses occur (Figure 6, Figure 1). The exact positions of the streams migrate laterally between the different years, i.e. meltwater channels are not being reactivated over the course of several summers. Further down-glacier the meltwater catchments are laterally confined to the trough between the moraine ridges, and thus the stream locations remain similar between the different years (Figure 6). Field visits in 2016-2018 showed that these streams became reactivated every year. Some of them drained into new moulins a few metres further up-glacier of the previous year´s moulins, which later become relict and close through ice deformation over the following years. Others are directly connected to the large-scale erosion features of the high-relief zone (cryo-valleys).

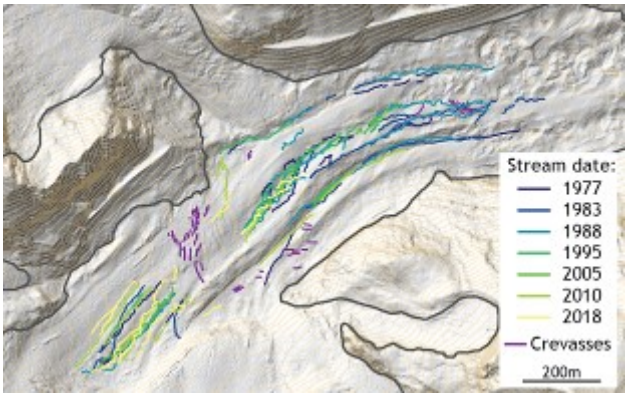

Figure 6: Supraglacial streams as mapped for different dates. The background is composed of a hillshade of the 2018 DEM (spatial resolution 2 m) and 20 m contour lines.

4.4. High-relief zone

Glacier surface morphology in the high-relief zone yields an unstructured pattern of relatively small-scale topographic highs and lows. The main visible patterns are meander-like channel features, which we term cryo-valleys. These features are no longer aligned with the ice flow but appear oriented in all directions. Their lateral slopes are steep and often exhibit ice cliffs. Debris cones – debris-covered ice mounds (cf. Boulton 1967, Goodsell et al. 2005) – have formed and a heterogeneous debris distribution has developed with large boulders in the depressions (supplementary Figure 7). Erosion features could not be mapped for 1946 and 1961 due to partial snow cover on the tongue. The total area of the high-relief zone decreased between 1977 and 1988, but has strongly grown after 1995 to reach about 0.6 km² in 2018 (Figure 7), i.e. covering approximately 4% of the total glacier surface and approximately 7% of the ablation area. Similarly, the total volume of the erosion features has at first slightly decreased but has subsequently quintupled from $<1*10^6$ m³ to almost $5*10^6$ m³ (Figure 7).

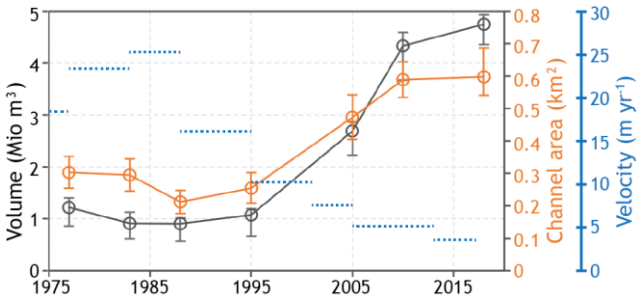

Figure 7: Evolution of high-relief erosion feature volume (black curve) and area (orange curve) as well as average velocity at the central and lower glacier tongue (blue dotted lines).

The multi-temporal analysis reveals that the high-relief zone is mainly the result of two large cryo-valleys that have persisted in the lowest part of the glacier tongue since 1977 and have grown in volume and area since 1995 (Figure 1). The orographic left cryo-valley is emerging from two main tributaries at approximately 800 m from the terminus. Its northern part appears at the prolongation

of the former tributary valley from Stockjigletscher and Schönbielgletscher. The southern part emerges downstream of the central glacier part, in the prolongation of the trough between ridges R1 and R2. The second (most southern) cryo-valley is smaller and less clearly pronounced (Figure 1). Both cryo-valleys changed in shape over each period of observation. In this zone, the moraine ridges that emerged up-stream in the low-relief area decrease in elevation and vanish, likely due to erosion by the combined action of meltwater erosion, cliff backwasting, and gravitational debris redistribution.

The contribution of the volume change at the erosion features to glacier-wide thinning over the period 2005-2010 equalled ~10 cm yr^{-1} (ablation area) and ~2 cm yr^{-1} (glacier-wide), respectively (see also supplementary Figure 6). This value does not exceed the DEM uncertainty and is quite small in comparison to the total observed elevation change rate, which is on the order of -1 m yr^{-1} glacier-wide (Mölg et al. 2019).

4.5. Hydraulic potential

If a distributed basal drainage system is assumed (see chapter 3.4), the across-flow surface topography in the low-relief area is dominant for the hydraulic potential across-glacier, especially in hydraulic transects HT2 and HT3 (Figure 8), despite considerable bed undulations. The small medial moraine ridges of several metres to tens of metres height constitute lateral barriers that are too big to overcome by the water flowing at the glacier bed and likely also englacially. When considering the general along-flow slope of the glacier bed of approximately 5°, it seems unlikely that the englacial or subglacial flow paths will change subcatchments confined by the along-flow medial moraines at the surface.

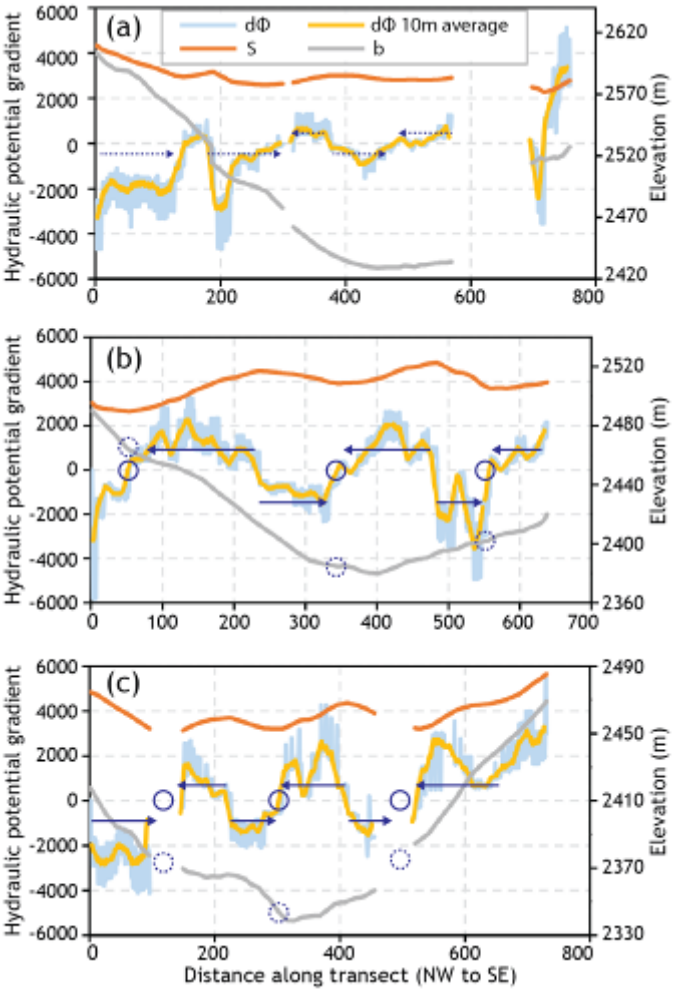

Figure 8: Gradient of the hydraulic potential (yellow and blue lines) across three glacier transects, HT1 (a), HT2 (b), HT3 (c) together with the surface (orange lines) and the bed cross profiles (grey lines; see Figure 1 for the location of the transects). Blue arrows mark the potential flow direction of the water away from the along-flow direction at the glacier bed and towards the circles at positions of a zero gradient in hydraulic potential (depression in hydraulic potential) and dashed circles indicate the corresponding position at the glacier bed. Arrows in (a) are dashed due to the low absolute values of the hydraulic potential.

4.6. Ice cliff formation

The formation of ice cliffs is closely related to the location of cryo-valleys and the high-relief area. Both in 2005 and in 2018, approximately 75% of all ice cliffs were located inside the high-relief erosion features. From the remaining cliff area, 12% (2005) and 15% (2018) existed at the glacier margins, mostly at the terminus and on the lateral margin of Schönbielgletscher (SBG, Figure 1). The terminal ice cliffs develop from slumping of debris at the oversteepened slopes of the glacier mouth, likely due to continuous ice erosion and debris evacuation by the river. At Schönbielgletscher steep slopes have developed on its western lateral margin where the debris-free Stockjigletscher branch one has strongly thinned during recent decades, in contrast to its debris-covered neighbour. The

remaining 10-15% of ice cliffs were observed at calving fronts at small ponds, crevasses and fractures around collapsing roofs of englacial voids.

4.7. Evolution of the high-relief area

As an example of a meander of the left cryo-valley, we show how a high-relief area develops out of the originally smooth glacier surface over a period of two decades (Figure 9). At first, a meltwater stream incises into the ice and small ice cliffs develop at the slopes (1988). The stream incises further and its meanders become more pronounced while the ice cliff area keeps growing (1995). From 1999 onwards, ice cliffs cover most of the lateral meander slopes, which leads to an enlarging of the meander feature by ice cliff backwasting in various directions (2001). Over time, this process significantly increases the area of the erosion feature (2005) and encompasses complex patterns of debris redistribution from outside the erosion feature (ice cliff backwasting) and from within (fluvial transport, ice cliff backwasting). In 2007, the backwasting of ice cliffs led to the unification of the two cryo-valleys on the left glacier side, and a large hummocky surface was left behind (Figure 9). This example shows that it is possible to turn the relatively smooth, original glacier surface into an area of high relief with an incised stream, local depressions, heterogeneous debris distribution, and steep, ice-cliffed slopes facing in all directions, within a period of only a couple of decades.

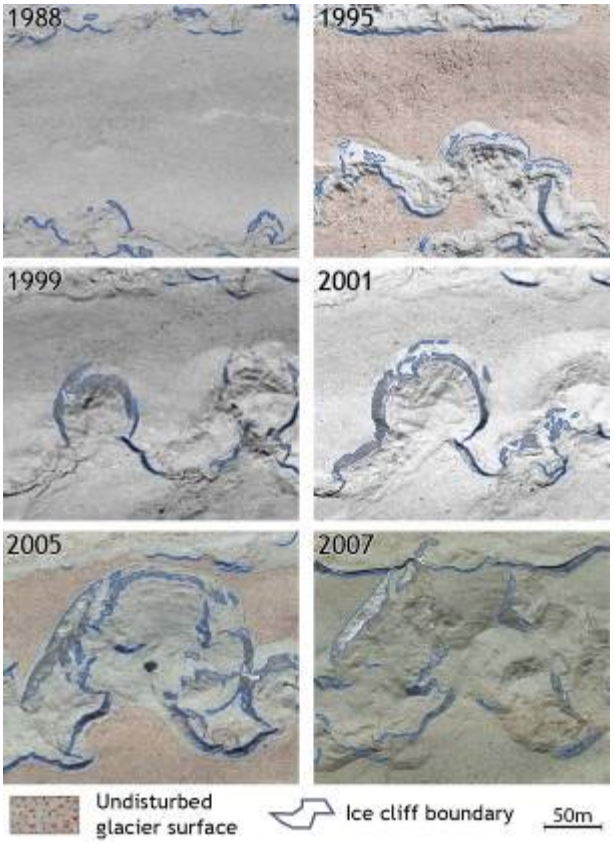

Figure 9: Time series of orthophotos documenting the evolution of two meanders over the course of twelve years. The clearly defined channel area from 1995 evolves into a high-relief zone where most of the originally smooth glacier surface becomes

reworked. Undisturbed glacier surfaces are only available for 1995 and 2005. The course of the stream becomes englacial over time.

5. Interpretation

The evolution of the different zones along the glacier tongue and their corresponding main features are tightly interlinked (Figure 10a) and developments in the upper zone directly influence the lower zones. Therefore we focus on this succession of processes and surface developments (Table 2) documented by the multi-temporal analysis.

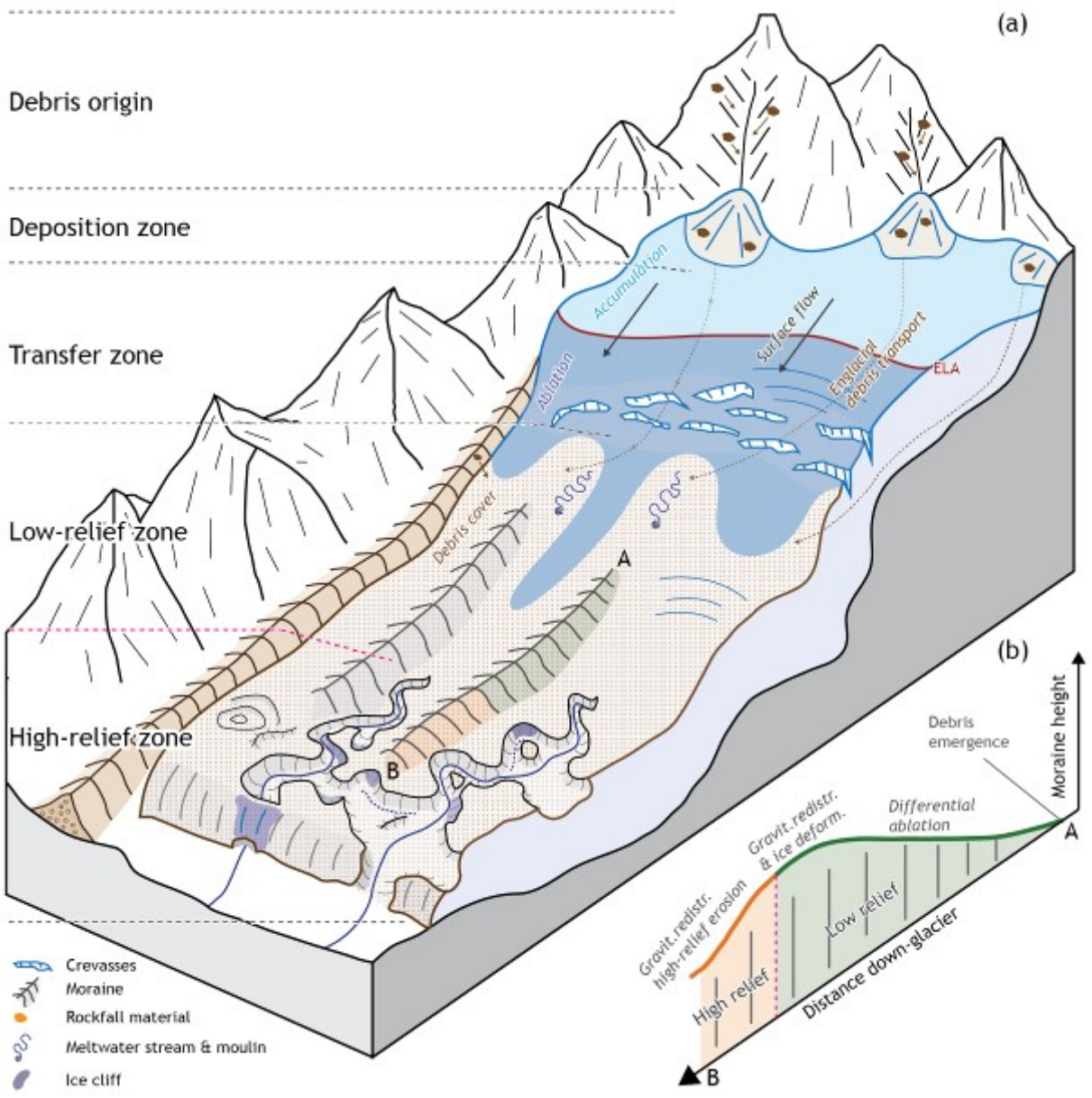

Figure 10: (a): Main elements and succession of zones on a debris-covered glacier. (b): Concept of medial moraine height evolution down-glacier and over time.

Table 2: Summary of the major landforms and processes in the discussed glacier zones.

Glacier zone	Major landforms	Main processes

Debris-free ablation zone	Homogeneous, smooth surface, crevasses at steeper sections	Ablation, plastic ice flow, non-plastic at crevasses
Low-relief zone	Medial moraines	Differential ablation, stream incision, debris redistribution
High-relief zone	Medial moraines, cryo-valleys, large-scale erosion features	Same as in low-relief zone, additionally ice cliff backwasting, cut-and-closure of incised streams

460

461 **5.1. Evolution of the low-relief zone and medial moraines**

462 Between the end of the LIA and the mid-20th century the glacier surface of the low-relief zone in the
463 upper part of the tongue turned from a smooth, slightly undulating surface into one being dominated
464 by along-flow ridges and troughs of a few metres to several tens of metres in height. Their formation
465 started in the transition zone from a debris-free to a debris-covered glacier surface and was driven by
466 local emergence of debris. Where such debris bands first emerged, the ablation rates decreased
467 creating contrasting thinning that shaped the medial moraines and the adjacent along-flow troughs
468 over time. The debris originates from rockfall at the headwalls surrounding the accumulation area
469 and the moraines can be classified as ablation dominated according to the classification by Eyles and
470 Rogerson (1978). The central moraine (R2) has turned from an ablation-dominated type to an
471 avalanche-type moraine (Eyles and Rogerson 1978) due to the rise of the ELA above the avalanche
472 cone locations. While the moraines grew down-glacier, the troughs in between remained debris-free
473 for a distance of between several hundred metres and two kilometres. The debris-free bands
474 narrowed due to further melt-out of englacial debris and debris redistribution from the slopes of the
475 moraines as proposed by previous studies (e.g. Small and Clark 1974, Eyles and Rogerson 1978, Vere
476 and Benn 1989).

477 Moraine height generally increases down-glacier as the ablation contrast accumulates and is well
478 reproduced by the simple numerical model that includes debris thickness dependent ablation.
479 However, further down-glacier we observed a stagnation in moraine height and even a decrease as
480 sketched out in the conceptual Figure 10b. This phenomenon was observed before and was
481 explained by (i) the complete melt-out of the vertical debris-containing ice column and (ii) the lateral
482 redistribution of debris together with ice deformation towards the steep moraine slopes (Eyles and
483 Rogerson 1978, Small and Clark 1974, Gomez and Small 1985, Bozhinskiy et al. 1986, Brook et al.
484 2017). In other words, the moraine height is self-limiting due to these processes, whereas it would
485 grow infinitely otherwise (Figure 5c). Explanation (i) is applicable for so-called ice-stream interaction
486 moraines (cf. Eyles and Rogerson 1978), i.e. medial moraines developing below the convergence of
487 tributaries, and where folding has occurred at the convergence of tributaries (Hambrey et al. 1999,
488 Appleby et al. 2010, Jennings et al. 2014). However, the complete melt-out of the debris column
489 below the confluence of large glacier branches (which we consider unlikely) would lead to moraine

height decrease rather than stagnation. Explanation (ii) is supported by our observations from the field (e.g. supplementary Figure 7) and the orthophotos, which indicate a widening of the debris cover at the moraines and the redistribution of large boulders away from the moraine ridges. The modelling including debris redistribution also reproduced this stagnation by achieving some sort of equilibrium between debris melt-out and redistribution (although neglecting stream incision, which would again contribute to moraine height decrease). A further process that may also limit the moraine height growth (and that was not considered in the modelling) is the across-flow ice deformation when the moraine is sufficiently high. Such moraine deformation under its own weight has been documented by differential GPS-measurements on the medial moraine of Unteraargletscher (Helbing 2006) and there it occurred at a moraine height around 20 m.

However, for interpreting observations of moraine height, we should also consider the potential influence of the glacier and hence the climate history. Our simple modelling suggests that during cooler climates the location of peak moraine height is further down-glacier than during warmer climates. The reasons are the lower position of the ELA and the smaller ablation contrasts due to smaller absolute ablation rates (Shroder et al. 2000). This may also be a relevant effect when interpreting the moraine heights of Zmuttgletscher, because the climate was cooler at the end of the LIA as well as during the 1920s and 1970s (Schmidli 2000, Hirschi et al. 2013). Assuming average flow velocities at the tongue of 30 m yr^{-1} (Mölg et al. 2019), the ice at the lowest transect (ST4) is 100-150 years old. Thus the ice and surface debris there likely date back to the 19^{th} century and have experienced more of the cooler periods, which may have reduced moraine growth over time. An additional factor (not accounted for in the model) for less strong moraine growth in ice originating from cooler periods is a lower debris concentration than today due to higher accumulation volumes and lower weathering rates (e.g. Glazyrin 1975, Kirkbride and Deline 2013, Bosson et al. 2015). Given the increasingly negative mass balance of many glaciers worldwide (Zemp et al. 2019), this effect likely plays a widespread role. The model results yield maximum moraine heights of approximately 25 m, similar to the observed values and literature findings (e.g. Eyles and Rogerson 1978, Small and Clark 1974, Brook et al. 2017). Thus, we suggest that the model parameters and across-profile contrasts in debris concentration represent a good approximation of reality.

Note that moraine height decreased at all transects in the period 1977-1988 (Figure 10b) which is coincident with periods of increased flow velocities induced by additional mass flux (Mölg et al. 2019). In the area of the transects, the more prominent parts of the medial moraines were pushed further down-glacier and replaced by less developed parts from further up-glacier. At the same time, reduced ablation attenuated the process of differential ablation while diffusion processes continued

to act. The height increase at ST2 (1983-2017) and at ST3 (1995-2010) is almost linear (R^2=0.89/0.95), which is in line with our modelling results and the modelling study by Anderson (2000).

Debris emergence moved up-glacier over time, together with continued negative mass balance and a rise of the ELA. As the ELA approaches debris deposition locations, englacial travel distances shorten and the debris emerges further up-glacier (e.g. Boulton 1978). With a rise of the climatic ELA of about 300 m during the second half of the 20th century, the central flow unit of Zmuttgletscher has turned into an avalanche-type glacier (cf. Eyles and Rogerson 1978, Vere and Benn 1989). Thus, the flow unit below Dent d'Hérens is now primarily nourished by avalanching and the debris cover starts close to the foot of the wall. Therefore, the central and most prominent moraine ridge (R2) now develops in the highest transect just below the icefall (ST1), only a few hundred metres from where the deposition takes place.

The moraine evolution model has been tuned for Zmuttgletscher with parameters within the range of literature values (e.g. Bozhinskiy et al. 1986, Anderson 2000), therefore the model results are – at the moment – limited to Zmuttgletscher. Nevertheless the model is applicable to investigate medial moraines at other glaciers, but is based on assumptions of debris concentration in the ice.

5.2. Surface morphology influences meltwater

The formation of along-flow ridges affects the meltwater that is produced on the glacier surface. Flat debris-covered areas tend to have relatively small catchments and thus small streams (Benn et al. 2017, Fyffe et al. 2019). The flat upper part of the low-relief zone of Zmuttgletscher, with no or relatively thin debris cover (mostly <15 cm), hosts comparatively small and laterally migrating supraglacial streams. A number of moulins and crevasses drain these streams at the down-glacier end of this flat area. As the moraine ridges develop further down-glacier, the supraglacial meltwater streams get strongly confined by these ridges and persistently follow the surface troughs in between. This means the ridges also constrain the streams to a few along-flow basins that drain relatively large catchments (Figure 6; Small and Clark 1974). This focussing of meltwater into a few along-flow streams with substantial meltwater discharge is essential for stream incision, which is mainly controlled by river discharge, the slope of the stream, and the ablation rate of the adjacent ice (Fountain and Walder 1998, Jarosch and Gudmundsson 2012).

En- and subglacially, the hydraulic gradient is also governed by the surface topography and hence by ridges and troughs, in particular before an efficient channelised drainage system is established. As the moraines develop along the glacier due to the emergence of debris they become high enough to direct any en- and subglacial water flow towards the positions of the troughs that had formed between the moraines (Figure 8). Thus, the meltwater flow is strongly confined by the moraines –

both supra- and subglacially. Once a channelised system is established, it is likely to persist given the conditions of negative mass balance and decreased glacier flow dynamics (e.g. Clayton 1964, Thompson et al. 2016).

5.3. Formation and relevance of the high-relief zone

The earliest aerial photograph from 1930 already shows distinct erosion features in the lowest, debris-covered part of the tongue (supplementary Figure 8). The analysis of the time series of orthoimages from 1946 onwards reveals that the initiation of the high-relief zone is a combined result of spatially persistent meltwater stream incision, subsequent debris redistribution and differential ablation.

5.3.1. Initiation of erosional features

Continuous meltwater stream incision and strong melting of the channel walls over several years can lead to small valleys on the glacier surface ('cryo-valleys'). On Zmuttgletscher, cryo-valley erosion features formed at the down-glacier prolongation of the meltwater streams that were confined by the moraine ridges (Figure 1, 10). Strongly reduced flow dynamics and increasingly negative mass balance since the 1980s support the flow path positions of the cryo-valleys over several decades. Debris is successively transported into the stream channels by gravitational redistribution from the adjacent glacier surface and fluvial transport from further up-glacier. Consequently, the debris is in parts of the channel bottoms often thicker than on the original, undisturbed glacier surface. The ablation contrast between the stream and the adjacent ice covered by thicker debris grows and supraglacial streams can further incise vertically by several metres. Due to their energy potential streams also continue to incise beneath the debris. If the stream channel is narrow enough, ice deformation is able to close the channel walls (Gulley et al. 2009), i.e. twice the horizontal velocity of a vertical ice cliff of 5-15 m height reaches values of up to 1 m per year (e.g. Jarosch and Gudmundsson 2012, Mercenier et al. 2018). In such cases the channel incision does not contribute to adjacent moraine height increase. During periods of strongly enhanced ablation, such cut-and-closure channels can become exposed again, as shown by Miles et al. (2017) for Lirung Glacier in Langtang Himalaya.

During periods of negative mass balance, englacially running water develops a strong erosive potential and plays an important role in the evolution of debris-covered glaciers during periods of negative mass balance (Clayton 1964, Krüger 1994, Janke et al. 2015, Thompson et al. 2016, Tanarro et al. 2019). If ice deformation during winter is not sufficient to close the conduit, large englacial voids can develop over time. Subsequent roof collapse can transform the void into a supraglacial

erosion feature. This effect could potentially play a role in the rapid down-glacier enlargement of the cryo-valleys on Zmuttgletscher but this was not fully conclusive from the data.

5.3.2. Conceptual high-relief area evolution

We showed that an incising stream can initiate a high-relief area on a debris-covered glacier tongue. Figure 11 conceptually summarises the main steps of this process, which we illustrated at one specific meander at Zmuttgletscher (Figure 9). Persistent supraglacial streams on a debris-covered glacier surface will likely incise into the ice and initiate a cryo-valley (e.g. Gulley et al. 2009). This is due to increased ice melt in the debris-free river bed as well as the erosion of ice and debris by the water flow, in contrast to the continuous debris cover adjacent to the flow channels, which attenuates melt rates. Streams on and within the ice can produce the observed sinuous channel shape (Gulley et al. 2009, Benn et al. 2017), similar to rivers in sedimentary flatlands (cf. Ikeda and Parker 1989). Steep slopes can form at the lateral margins of the cryo-valleys or by the collapse of an englacial void (Figure 11a). In certain places, these slopes steepen enough for the debris to slide off (Figure 11b). The sub-debris ice becomes exposed to the atmosphere and the cliff backwastes faster than the debris-covered surrounding slopes, with south-facing cliffs showing higher rates than north-facing ones (Figure 11c; e.g. Sakai et al. 2002, Reid and Brock 2014, Buri and Pellicciotti 2018). Due to the sinusoidal nature of streams, a cryo-valley often consists of pronounced meanders, and thus ice cliffs can face any direction. As a result, the backwasting process can affect the surroundings in all directions and widens the valley (Figure 11c). Because the valley bottom is also debris-covered, the stream continues to incise locally and a new valley can form. This succession of processes can, as in the case of Zmuttgletscher, lead to a topographical reshaping of the formerly smooth surface to a high-relief area with relief differences in the order of a few tens of metres (Figure 11d).

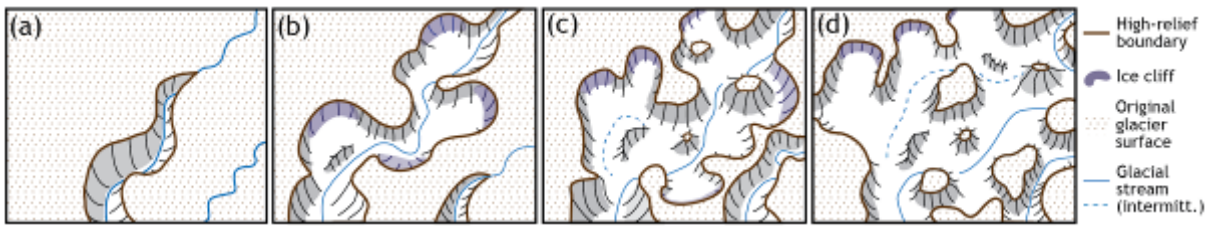

Figure 11: Conceptual model of the initiation and development of a high-relief zone from a supraglacial meltwater stream. Apart from the ice cliffs, all surfaces are debris covered, including the inside of the high-relief area.

Ice cliffs can backwaste rapidly due to their typically low albedo (see cliff colour in Figure 9; e.g. Buri et al. 2016). In mid-latitudes, backwasting rates can reach up to 5-15 m per summer, even higher than the ablation rates on debris-free ice at similar elevations, and also higher than annual flow velocities in the lower part of Zmuttgletscher (e.g. Röhl 2008, Han et al. 2010, Brun et al. 2016, Watson et al. 2017, Mölg et al. 2019). Both decreasing flow dynamics and increasing temperatures

leading to higher discharge enforce the enlargement of the high-relief zone, and affected areas can expand further up-glacier. Vice versa, the decrease in high-relief area and volume before 1988 is likely due to an increase in flow velocities and a decrease in summer temperatures (Schmidli 2000, Bauder et al. 2007, Mölg et al. 2019).

5.3.3. Topographic inversion

Debris cover gets redistributed due to steep walls at backwasting ice cliffs. Large areas of original glacier surface relocate their debris onto a relatively small area at small valley meanders, which occur during the beginning of the backwasting process. As a consequence, the locally decreased ablation can induce the formation of debris cones (Figure 9 in 1999 and 2001). As in the example on Zmuttgletscher illustrated in Figure 12, this can lead to a topographic inversion where a former surface low becomes a topographic high (Figure 12). Over time, the elevation difference between the peak of the debris cone and its surroundings increases, represented by 2 m contour lines in the uphill and downhill direction in Figure 12a. With continuous glacier thinning, the glacier surface with the same elevation as the debris cone peak retreats further upstream, thus the local maximum becomes more pronounced (Figure 12b). The potential mechanism of topographic inversion on debris-covered glacier tongues has been mentioned before (Thompson et al. 2016, Nicholson et al. 2018), but has, to our knowledge, never been fully documented.

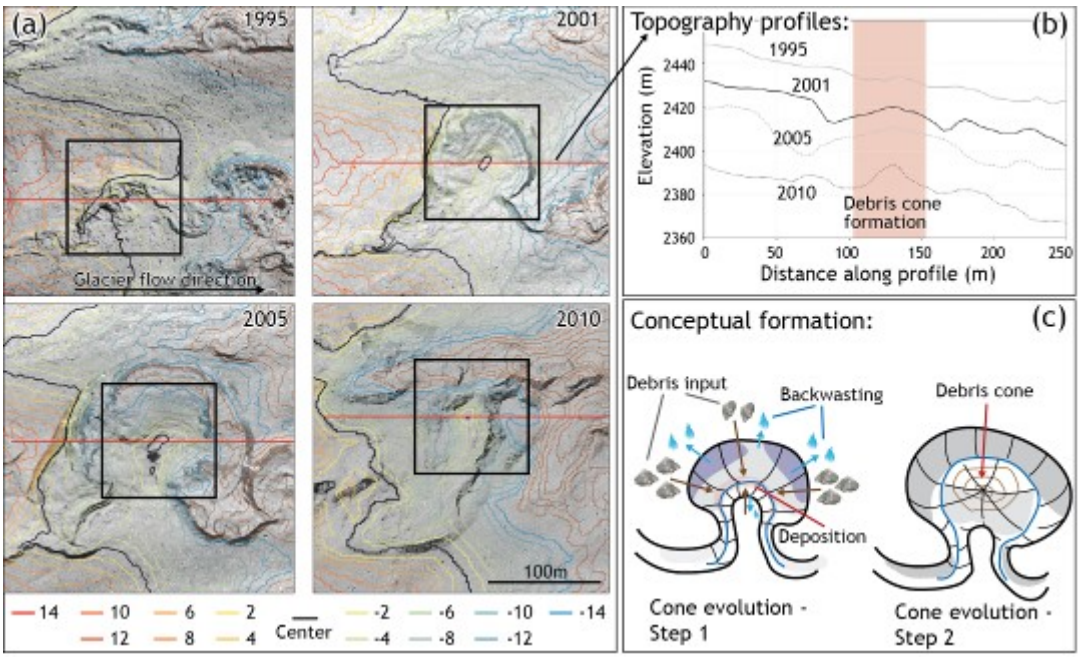

Figure 12: (a): Example of a topographic inversion. The contour lines are 2 m equidistant, centred around the highest point of the former meander centre, and cover 14 m of elevation difference both upstream and downstream of the centre. (b) Elevation profiles for the same dates with the debris cone in the centre. (c) Conceptual formation of the debris cone from a meander centre.

Other reasons for heterogeneous debris distribution apart from redistribution at cliffs and fluvial transport are englacial septa with various dip angles (e.g. Vere and Benn 1989, Appleby et al. 2010, Kirkbride and Deline 2013) as well as the melt-out of englacially transported and accumulated debris in conduits (Hooke et al. 1985, Kirkbride and Spedding 1996).

The action of these processes over decadal time scales, combined with thick debris cover and sluggish dynamics, seems to form a surface morphology that closely resembles that of well-studied heavily debris-covered glacier tongues in the Himalayas and that is difficult to backtrack (e.g. Watanabe et al. 1986, Iwata et al. 2000, Benn et al. 2017). Benn et al. (2017) reported an example of cryo-valley formation at the transition zone between smooth and high-relief area and its subsequent enlargement over time on Ngozumpa Glacier. Studying these transition zones at Himalayan glaciers over longer time periods could reveal similarities or differences to the concepts presented here and may improve the understanding of the genesis of the high-relief areas on such glaciers.

5.3.4. Glacier-wide importance of the high-relief zone

Volume loss of ~0.2-0.3*10^6 m^3 yr^{-1} is substantial in terms of discharge but less relevant considering the glacier-wide volume loss of almost 16*10^6 m^3 yr^{-1}. However, annual elevation change in the high-relief area can exceed -2 m yr^{-1} (2005-2017), which is two to three times higher than glacier-wide values. Thus, high-relief areas are important on a local scale also in the case of Zmuttgletscher. Average elevation changes at the lower tongue of nearby debris-free Findelgletscher are in the range of -5 m yr^{-1} (Joerg and Zemp 2014). Thus, we conclude that the influence of high-relief areas on the local volume change on the lower part of the tongue is considerable, but is compensated by debris insulation by a factor of 2-3. In light of thicker debris on many large debris-covered glaciers a similar or even higher compensation factor of debris cover can be expected.

5.4. Formation of ice cliffs

We showed that on Zmuttgletscher three quarters of all ice cliffs on the main tongue are located in the area of the erosion features. Also for most of the remaining – mostly marginal – ice cliffs the essential formation processes are linked to running water. This is in line with the formation processes for ice cliffs proposed by Benn et al. (2001) and Reid and Brock (2014), which also link them to meltwater action: supraglacial valley walls become oversteepened and debris slumping occurs. Subsidence at slowly collapsing englacial channels and calving at supraglacial ponds can also occur (e.g. Röhl 2008, Sakai et al. 2009) but is rare on Zmuttgletscher. Because the presence of moraine ridges influences both the stream location and the catchment, and hence the discharge (Benn et al. 2017), we conclude that the formation of ice cliffs is also a result of the surface morphology further up-glacier, which is dominated by the emergence location of supraglacial debris cover.

5.5. Relevance and implications

The presence of debris cover can significantly shape the surface morphology of a glacier. A succession of a smooth glacier surface, zones of low along-flow relief, and zones of high relief can form. Our observations of medial moraine formation and evolution are in line with observations from previous studies (Small and Clark 1974, Eyles and Rogerson 1978, Gomez and Small 1985). With our long-term analysis we showed that the uni-temporal shape of an along-flow moraine, as investigated in former studies, can also develop at one location over time. As glacier mass balance turns negative, debris cover emerges further up-glacier followed by the formation of a medial moraine, the prominence of which can increase and decrease again in the down-glacier direction and over time due to climatic changes, debris redistribution and ice deformation.

Ridge formation changes runoff paths and the accumulated meltwater can incise into the ice beneath a debris-covered glacier surface, thereby initiating the formation of small supraglacial valleys. The incision is likely to occur downstream of depressions between moraine ridges, where water accumulates both supra- and en/subglacially (cf. Arnold et al. 1998). The formation and enlarging of such cryo-valleys can be observed at various glaciers in the Alps, e.g. Oberaletschgletscher and Unteraargletscher in Switzerland and Glacier Noir (Écrins) in France (Vivian 1967, Deline 2002, Lardeux et al. 2016) and the Himalaya (Benn et al. 2017).

Zones of high relief are constantly changing, driven by strong contrasts of differential ablation and debris redistribution and erosion by meltwater, which has also been shown for Khumbu Glacier (Nepal; Iwata et al. 2000) and Hóladalsjökull (Iceland; Tanarro et al. 2019). Our study partly contrasts previous results stating that the high-relief zone and its features on debris-covered glaciers are relevant for the overall mass loss (e.g. Pellicciotti et al. 2015, Brun et al. 2016, Tanarro et al. 2019). In the case of Zmuttgletscher, the debris cover leads to reduced volume loss in the debris-covered area than can be expected on a similar debris-free glacier tongue, even when including the high-relief zone.

6. Conclusions

On Zmuttgletscher we find a down-glacier succession of morphological zones, from a smooth, low-relief zone with along-flow ridge structures to a zone of high relief in the lower glacier part with abundant ice cliffs. We found that the morphological evolution, zone formation and composition are strongly influenced and directed by the emergence pattern of supraglacial debris cover and the presence of locally concentrated meltwater.

Down-glacier of the debris bands that first emerged on the tongue of Zmuttgletscher, medial moraine ridges formed during the 20th century with a final prominence of up to 45 metres above the

surrounding terrain. Parallel to the glacier flow and in between the three main ridges, troughs formed in places that remained debris-free longer. Over time, ridge heights have increased and ridge onsets have moved up-glacier, due to continued negative mass balance and related debris cover expansion, supported by decreasing flow velocities. Increasing velocities in the 1970s/1980s led, in contrast, to a decrease in moraine height. We observed an attenuated height increase and even a decrease, down-glacier (in line with previous results) but also at one location over time. We show that moraine height is not only influenced by ice deformation and debris redistribution, but also by changes in climate, with slower moraine growth during cooler periods.

During their formation, the moraines start to force the meltwater to run in the troughs. Even englacially and subglacially, the surface morphology defines the lateral hydraulic gradient and prevents re-routing of the water perpendicular to the glacier flow. Supraglacially, the meltwater gets concentrated in the location of the troughs and this locally increased discharge leads to higher incision potential of the streams, eventually resulting in the formation of supraglacial valleys in the down-glacier prolongation of the troughs. Once initiated, these cryo-valleys can enlarge radially by hundreds of metres within a few decades and can thus form a zone of high topographic relief in the lower part of the glacier tongue. The enlargement of these erosion features is mainly driven by cliff backwasting at steep valley slopes and enforced by decreasing ice dynamics. On Zmuttgletscher, these processes have led to a growth in total erosion volume by a factor of five since the 1980s. The conceptual model of a transition from smooth debris cover (with elongated moraine ridges) to the formation of cryo-valleys and eventually high-relief zones with ice cliffs can well be seen at Zmuttgletscher: about 75% of the total cliff area is located inside the high-relief perimeter. Over longer time periods, these processes can be responsible for a complete reshaping of the originally smooth glacier surface into high-relief areas, as found on many debris-covered glaciers, especially in the Himalaya. Nevertheless, we found that the effect of the erosion features is locally important in the zone where most ice cliffs occur, but small compared to the average glacier-wide thinning rates for the same periods.

By studying the long-term evolution of the surface morphology of Zmuttgletscher, we provided insights into its importance for the glacier's evolution and showed its relevance for glacier models. The overall negative mass balance leads to an increasing relevance of debris-related changes in glacier surface morphology. In addition, the methods used in this paper are transferable to other glaciers, which may help to gain a more general understanding of how debris-covered glaciers evolve over longer time periods. For glaciers that carry large amounts of debris, such considerations will also be helpful in interpreting post-glacial debris volumes and distributions as well as questions on sediment transfer and storage.

Acknowledgements

This study was funded by the SNSF project #200021_169775 “Understanding and quantifying the transient dynamics and evolution of debris-covered glaciers”. We greatly appreciate the provision of the ice thickness data by A. Bauder and the VAW group (ETH Zurich), which were collected in the framework of Glacier Monitoring in Switzerland, GLAMOS. Debris thickness measurements were conducted and supported by R. Ganarin, A. Cicoira and M. Schulthess. The UAV campaign was supported by A. Cicoira.

Author contribution statement

All authors contributed to the design of the study and the final version of the manuscript. DEM production and all observation-based analysis were accomplished by N.M. J.F. developed and described the moraine evolution model. Debris thickness measurements and UAV imagery were gathered by N. Mölg and a volunteering colleague.

Publication bibliography

Agisoft LLC (2016): PhotoScan. Version 1.4: Agisoft.

Anderson, Leif S.; Anderson, Robert S. (2016): Modeling debris-covered glaciers. Response to steady debris deposition. In *The Cryosphere* 10 (3), pp. 1105–1124. DOI: 10.5194/tc-10-1105-2016.

Anderson, Leif S.; Anderson, Robert S. (2018): Debris thickness patterns on debris-covered glaciers. In *Geomorphology* 311, pp. 1–12. DOI: 10.1016/j.geomorph.2018.03.014.

Anderson, Robert S. (2000): A model of ablation-dominated medial moraines and the generation of debris-mantled glacier snouts. In *J. Glaciol.* 46 (154), pp. 459–469. DOI: 10.3189/172756500781833025.

Appleby, John R.; Brook, Martin S.; Vale, Simon S.; Macdonald-creevey, Amanda M. (2010): Structural glaciology of a temperate maritime glacier: lower fox glacier, new zealand. In *Geografiska Annaler: Series A, Physical Geography* 92 (4), pp. 451–467. DOI: 10.1111/j.1468-0459.2010.00407.x.

Arnold, Neil; Richards, Keith; Willis, Ian; Sharp, Martin (1998): Initial results from a distributed, physically based model of glacier hydrology. In *Hydrol. Process.* 12 (2), pp. 191–219. DOI: 10.1002/(SICI)1099-1085(199802)12:2<191::AID-HYP571>3.0.CO;2-C.

Bauder, Andreas; Funk, Martin; Huss, Matthias (2007): Ice-volume changes of selected glaciers in the Swiss Alps since the end of the 19th century. In *Ann. Glaciol.* 46, pp. 145–149. DOI: 10.3189/172756407782871701.

Benn, D. I.; Bolch, T.; Hands, K.; Gulley, J.; Luckman, A.; Nicholson, L. I. et al. (2012): Response of debris-covered glaciers in the Mount Everest region to recent warming, and implications for outburst flood hazards. In *Earth-Science Reviews* 114 (1-2), pp. 156–174. DOI: 10.1016/j.earscirev.2012.03.008.

Benn, D. I.; Wiseman, S.; Hands, K. A. (2001): Growth and drainage of supraglacial lakes on debris-mantled Ngozumpa Glacier, Khumbu Himal, Nepal. In *J. Glaciol.* 47 (159), pp. 626–638. DOI: 10.3189/172756501781831729.

Benn, Douglas I.; Thompson, Sarah; Gulley, Jason; Mertes, Jordan; Luckman, Adrian; Nicholson, Lindsey (2017): Structure and evolution of the drainage system of a Himalayan debris-covered glacier, and its relationship with patterns of mass loss. In *The Cryosphere* 11 (5), pp. 2247–2264. DOI: 10.5194/tc-11-2247-2017.

Bolch, T.; Kulkarni, A.; Kääb, A.; Huggel, C.; Paul, F.; Cogley, J. G. et al. (2012): The state and fate of Himalayan glaciers. In *Science (New York, N.Y.)* 336 (6079), pp. 310–314. DOI: 10.1126/science.1215828.

Bosson, Jean-Baptiste; Deline, Philip; Bodin, Xavier; Schoeneich, Philippe; Baron, Ludovic; Gardent, Marie; Lambiel, Christophe (2015): The influence of ground ice distribution on geomorphic dynamics since the Little Ice Age in proglacial areas of two cirque glacier systems. In *Earth Surf. Process. Landforms* 40 (5), pp. 666–680. DOI: 10.1002/esp.3666.

Boulton, G. S. (1967): The Development of a Complex Supraglacial Moraine at the Margin of Sørbreen, Ny Friesland, Vestspitsbergen. In *J. Glaciol.* 6 (47), pp. 717–735. DOI: 10.3189/S0022143000019961.

Boulton, G. S. (1978): Boulder shapes and grain-size distributions of debris as indicators of transport paths through a glacier and till genesis. In *Sedimentology* 25 (6), pp. 773–799. DOI: 10.1111/j.1365-3091.1978.tb00329.x.

Bozhinskiy, A. N.; Krass, M. S.; Popovnin, V. V. (1986): Role of Debris Cover in the Thermal Physics of Glaciers. In *J. Glaciol.* 32 (111), pp. 255–266. DOI: 10.3189/S0022143000015598.

Brook, Martin; Hagg, Wilfried; Winkler, Stefan (2017): Contrasting medial moraine development at adjacent temperate, maritime glaciers: Fox and Franz Josef Glaciers, South Westland, New Zealand. In *Geomorphology* 290, pp. 58–68. DOI: 10.1016/j.geomorph.2017.04.015.

Brun, Fanny; Buri, Pascal; Miles, Evan S.; Wagnon, Patrick; Steiner, Jakob; Berthier, Etienne et al. (2016): Quantifying volume loss from ice cliffs on debris-covered glaciers using high-resolution terrestrial and aerial photogrammetry. In *J. Glaciol.* 62 (234), pp. 684–695. DOI: 10.1017/jog.2016.54.

Buri, Pascal; Pellicciotti, Francesca (2018): Aspect controls the survival of ice cliffs on debris-covered glaciers. In *Proceedings of the National Academy of Sciences of the United States of America* 115 (17), pp. 4369–4374. DOI: 10.1073/pnas.1713892115.

Buri, Pascal; Pellicciotti, Francesca; Steiner, Jakob F.; Miles, Evan S.; Immerzeel, Walter W. (2016): A grid-based model of backwasting of supraglacial ice cliffs on debris-covered glaciers. In *Ann. Glaciol.* 57 (71), pp. 199–211. DOI: 10.3189/2016AoG71A059.

Clayton, Lee (1964): Karst Topography on Stagnant Glaciers. In *J. Glaciol.* 5 (37), pp. 107–112. DOI: 10.3189/S0022143000028628.

Deline, Philip (2002): Etude géomorphologique des interactions écroulements rocheux/glaciers dans la haute montagne alpine (versant sud-est du massif du Mont Blanc). PhD thesis. Université de Savoie, Chambery. Géographie.

eCognition Essentials 1.3. Version 2 (2016): Trimble Germany GmbH. Available online at http://www.ecognition.com/.

Eyles, N.; Rogerson, R. J. (1978): A Framework for the Investigation of Medial Moraine Formation: Austerdalsbreen, Norway, and Berendon Glacier, British Columbia, Canada. In *J. Glaciol.* 20 (82), pp. 99–113. DOI: 10.3189/S0022143000021249.

Fountain, A. G.; Walder, J. S. (1998): Water flow through temperate glaciers. In *Reviews of Geophysics* 36 (3), pp. 299–328.

Fyffe, C. L.; Brock, B. W.; Kirkbride, M. P.; Mair, D.W.F.; Arnold, N. S.; Smiraglia, C. et al. (2019): Do debris-covered glaciers demonstrate distinctive hydrological behaviour compared to clean glaciers? In *Journal of Hydrology* 570, pp. 584–597. DOI: 10.1016/j.jhydrol.2018.12.069.

GLAMOS (2018): Swiss glacier monitoring network. Available online at http://swiss-glaciers.glaciology.ethz.ch/index.html, checked on 12/7/2018.

Glazyrin, G. E. (1975): The formation of ablation moraines as a function of the climatological environment. In IAHS (Ed.): Snow and Ice - Symposium - Neiges et Glaces. Proceedings of the Moscow Symposium, August 1971, vol. 104. IAHS-AISH (104), pp. 106–110.

Gomez, B.; Small, R. (1985): Medial Moraines of the Haut Glacier D'arolla, Valais, Switzerland: Debris Supply and Implications For Moraine Formation. In *J. Glaciol.* 31 (109), pp. 303–307. DOI: 10.3189/S0022143000006638.

Goodsell, B.; Hambrey, M. J.; Glasser, N. F. (2005): Debris transport in a temperate valley glacier: Haut Glacier d'Arolla, Valais, Switzerland. In *J. Glaciol.* 51 (172), pp. 139–146. DOI: 10.3189/172756505781829647.

Gulley, J. D.; Benn, D. I.; Müller, D.; Luckman, A. (2009): A cut-and-closure origin for englacial conduits in uncrevassed regions of polythermal glaciers. In *J. Glaciol.* 55 (189), pp. 66–80. DOI: 10.3189/002214309788608930.

Hambrey, Michael J.; Bennett, Matthew R.; Dowdeswell, Julian A.; Glasser, Neil F.; Huddart, David (1999): Debris entrainment and transfer in polythermal valley glaciers. In *J. Glaciol.* 45 (149), pp. 69–86. DOI: 10.3189/S0022143000003051.

Han, Haidong; Wang, Jian; Wei, Junfeng; Liu, Shiyin (2010): Backwasting rate on debris-covered Koxkar glacier, Tuomuer mountain, China. In *J. Glaciol.* 56 (196), pp. 287–296. DOI: 10.3189/002214310791968430.

Helbing, Jakob (2006): Glacier dynamics of Unteraargletscher: Verifying theoretical concepts through flow modeling. PhD Thesis. ETH Zürich, Zürich. Versuchsanstalt für Wasserbau. Available online at https://ethz.ch/content/dam/ethz/special-interest/baug/vaw/vaw-dam/documents/das-institut/mitteilungen/2000-2009/196.pdf, checked on 8/25/2019.

Herreid, Sam; Pellicciotti, Francesca (2018): Automated detection of ice cliffs within supraglacial debris cover. In *The Cryosphere* 12 (5), pp. 1811–1829. DOI: 10.5194/tc-12-1811-2018.

Hirschi, E.; Auchmann, R.; Martius, O.; Brönnimann, S. (2013): The 1945-1949 droughts in Switzerland. In S. Brönnimann, O. Martius (Eds.): Weather extremes during the past 140 years. Bern (Geographica Bernensia, G89), pp. 81–90.

Hooke, Roger L; Wold, B; Hagen, J. O. (1985): Subglacial hydrology and sediment transport at Bondhusbreen, southwest Norway. In *Geol Soc America Bull* 96 (3), p. 388. DOI: 10.1130/0016-7606(1985)96<388:SHASTA>2.0.CO;2.

Ikeda, Syunsuke; Parker, Gary (1989): River Meandering. Washington, D. C.: American Geophysical Union (12).

Iwata, S.; Aoki, T.; Kadota, T.; Seko, K.; Yamaguchi, S. (2000): Morphological evolution of the debris cover on Khumbu Glacier, Nepal, between 1978 and 1995. In Masayoshi Nakawo, C. F. Raymond, A. Fountain (Eds.): Debris-covered glaciers. Proceedings of an international workshop held at the University of Washington in Seattle, Washington, USA, 13-15 September 2000 / edited by M. Nakawo, C.F. Raymond, A. Fountain. Wallingford, Oxfordshire: IAHS (IAHS publication, no.264), pp. 3–13.

Iwata, Shuji; Watanabe, Okitsugu; Fushimi, Hiroji (1980): Surface Morphology in the Ablation Area of the Khumbu Glacier. In *Journal of the Japanese Society of Snow and Ice* 41 (Special), pp. 9–17. DOI: 10.5331/seppyo.41.Special_9.

Janke, Jason R.; Bellisario, Antonio C.; Ferrando, Francisco A. (2015): Classification of debris-covered glaciers and rock glaciers in the Andes of central Chile. In *Geomorphology* 241, pp. 98–121. DOI: 10.1016/j.geomorph.2015.03.034.

Jarosch, A. H.; Gudmundsson, M. T. (2012): A numerical model for meltwater channel evolution in glaciers. In *The Cryosphere* 6 (2), pp. 493–503. DOI: 10.5194/tc-6-493-2012.

Jennings, Stephen J.A.; Hambrey, Michael J.; Glasser, Neil F. (2014): Ice flow-unit influence on glacier structure, debris entrainment and transport. In *Earth Surf. Process. Landforms* 39 (10), pp. 1279–1292. DOI: 10.1002/esp.3521.

Joerg, Philip Claudio; Zemp, Michael (2014): Evaluating volumetric glacier change methods using airborne laser scanning data. In *Geografiska Annaler: Series A, Physical Geography* 96 (2), pp. 135–145. DOI: 10.1111/geoa.12036.

Juen, M.; Mayer, C.; Lambrecht, A.; Han, H.; Liu, S. (2014): Impact of varying debris cover thickness on ablation. A case study for Koxkar Glacier in the Tien Shan. In *The Cryosphere* 8 (2), pp. 377–386. DOI: 10.5194/tc-8-377-2014.

Kirkbride, Martin; Spedding, Nick (1996): The influence of englacial drainage on sediment-transport pathways and till texture of temperate valley glaciers. In *Ann. Glaciol.* 22, pp. 160–166. DOI: 10.3189/1996AoG22-1-160-166.

Kirkbride, Martin P. (1993): The temporal significance of transitions from melting to calving termini at glaciers in the central Southern Alps of New Zealand. In *The Holocene* 3 (3), pp. 232–240. DOI: 10.1177/095968369300300305.

Kirkbride, Martin P. (2002): Processes of glacial transportation. In : Modern and Past Glacial Environments: Elsevier, pp. 147–169.

Kirkbride, Martin P.; Deline, Philip (2013): The formation of supraglacial debris covers by primary dispersal from transverse englacial debris bands. In *Earth Surf. Process. Landforms* 38 (15), pp. 1779–1792. DOI: 10.1002/esp.3416.

Kraaijenbrink, P.D.A.; Shea, J. M.; Pellicciotti, F.; Jong, S. deM.; Immerzeel, W. W. (2016): Object-based analysis of unmanned aerial vehicle imagery to map and characterise surface features on a debris-covered glacier. In *Remote Sensing of Environment* 186, pp. 581–595. DOI: 10.1016/j.rse.2016.09.013.

Krüger, J. (1994): Glacial processes, sediments, landforms and stratigraphy in the terminus region of Myrdalsjökull, Iceland. In *Folia Geographica Danica* XXI (233).

Langhammer, Lisbeth; Rabenstein, Lasse; Schmid, Lino; Bauder, Andreas; Grab, Melchior; Schaer, Philipp; Maurer, Hansruedi (2019): Glacier bed surveying with helicopter-borne dual-polarization ground-penetrating radar. In *J. Glaciol.* 65 (249), pp. 123–135. DOI: 10.1017/jog.2018.99.

Lardeux, Pierre; Glasser, Neil; Holt, Tom; Hubbard, Bryn (2016): Glaciological and geomorphological map of Glacier Noir and Glacier Blanc, French Alps. In *Journal of Maps* 12 (3), pp. 582–596. DOI: 10.1080/17445647.2015.1054905.

Le Brocq, A. M.; Payne, A. J.; Siegert, M. J.; Alley, R. B. (2009): A subglacial water-flow model for West Antarctica. In *J. Glaciol.* 55 (193), pp. 879–888. DOI: 10.3189/002214309790152564.

Loomis, S. R. (1970): Morphology and structure of an ice-cored medial moraine, Kaskawulsh Glacier, Yukon. In S. R. Loomis, J. Dozier, K. J. Ewing (Eds.): Studies of Morphology and Stream Action on Ablating Ice: Arctic Inst. North America, pp. 1–56.

Mercenier, Rémy; Lüthi, Martin P.; Vieli, Andreas (2018): Calving relation for tidewater glaciers based on detailed stress field analysis. In *The Cryosphere* 12 (2), pp. 721–739. DOI: 10.5194/tc-12-721-2018.

Mihalcea, C.; Mayer, C.; Diolaiuti, G.; D'Agata, C.; Smiraglia, C.; Lambrecht, A. et al. (2008): Spatial distribution of debris thickness and melting from remote-sensing and meteorological data, at debris-

915 covered Baltoro glacier, Karakoram, Pakistan. In *Ann. Glaciol.* 48, pp. 49–57. DOI:
916 10.3189/172756408784700680.

917 Miles, Evan S.; Steiner, Jakob; Willis, Ian; Buri, Pascal; Immerzeel, Walter W.; Chesnokova, Anna;
918 Pellicciotti, Francesca (2017): Pond Dynamics and Supraglacial-Englacial Connectivity on Debris-
919 Covered Lirung Glacier, Nepal. In *Front. Earth Sci.* 5, p. 156. DOI: 10.3389/feart.2017.00069.

920 Mölg, Nico; Bolch, Tobias (2017): Structure-from-Motion Using Historical Aerial Images to Analyse
921 Changes in Glacier Surface Elevation. In *Remote Sensing* 9 (10), p. 1021. DOI: 10.3390/rs9101021.

922 Mölg, Nico; Bolch, Tobias; Rastner, Philipp; Strozzi, Tazio; Paul, Frank (2018): A consistent glacier
923 inventory for Karakoram and Pamir derived from Landsat data: distribution of debris cover and
924 mapping challenges. In *Earth Syst. Sci. Data* 10 (4), pp. 1807–1827. DOI: 10.5194/essd-10-1807-2018.

925 Mölg, Nico; Bolch, Tobias; Walter, Andrea; Vieli, Andreas (2019): The role of debris cover in the
926 evolution of Zmuttgletscher, Switzerland, since the end of the Little Ice Age. In *The Cryosphere*
927 *Discuss.*, pp. 1–34. DOI: 10.5194/tc-2018-292.

928 Nakawo, M.; Iwata, S.; Watanabe, O.; Yoshida, M. (1986): Processes which Distribute Supraglacial
929 Debris on the Khumbu Glacier, Nepal Himalaya. In *Ann. Glaciol.* 8, pp. 129–131. DOI:
930 10.3189/S0260305500001294.

931 Nicholson, Lindsey; Benn, Douglas I. (2006): Calculating ice melt beneath a debris layer using
932 meteorological data. In *J. Glaciol.* 52 (178), pp. 463–470. DOI: 10.3189/172756506781828584.

933 Nicholson, Lindsey I.; McCarthy, Michael; Pritchard, Hamish D.; Willis, Ian (2018): Supraglacial debris
934 thickness variability: impact on ablation and relation to terrain properties. In *The Cryosphere* 12 (12),
935 pp. 3719–3734. DOI: 10.5194/tc-12-3719-2018.

936 Østrem, G. (1959): Ice Melting under a Thin Layer of Moraine, and the Existence of Ice Cores in
937 Moraine Ridges. In *Geografiska Annaler* 41 (4), pp. 228–230.

938 Otto, J.-Chr.; Dikau, R. (2004): Geomorphologic system analysis of a high mountin valley in the Swiss
939 Alps. In *Zeitschrift für Geomorphologie* 48 (3), pp. 323–341.

940 Paul, F.; Barrand, N. E.; Baumann, S.; Berthier, E.; Bolch, T.; Casey, K. et al. (2013): On the accuracy of
941 glacier outlines derived from remote-sensing data. In *Ann. Glaciol.* 54 (63), pp. 171–182. DOI:
942 10.3189/2013AoG63A296.

943 Pellicciotti, Francesca; Stephan, Christa; Miles, Evan; Herreid, Sam; Immerzeel, Walter W.; Bolch,
944 Tobias (2015): Mass-balance changes of the debris-covered glaciers in the Langtang Himal, Nepal,
945 from 1974 to 1999. In *J. Glaciol.* 61 (226), pp. 373–386. DOI: 10.3189/2015JoG13J237.

946 Pix4D (2016): Pix4Dmapper pro: Pix4D.

947 Ragettli, Silvan; Bolch, Tobias; Pellicciotti, Francesca (2016): Heterogeneous glacier thinning patterns
948 over the last 40 years in Langtang Himal, Nepal. In *The Cryosphere* 10 (5), pp. 2075–2097. DOI:
949 10.5194/tc-10-2075-2016.

950 Reid, T. D.; Brock, B. W. (2014): Assessing ice-cliff backwasting and its contribution to total ablation
951 of debris-covered Miage glacier, Mont Blanc massif, Italy. In *J. Glaciol.* 60 (219), pp. 3–13. DOI:
952 10.3189/2014JoG13J045.

953 Röhl, Katrin (2008): Characteristics and evolution of supraglacial ponds on debris-covered Tasman
954 Glacier, New Zealand. In *J. Glaciol.* 54 (188), pp. 867–880. DOI: 10.3189/002214308787779861.

Sakai, A.; Nakawo, M.; Fujita, K. (2002): Distribution Characteristics and Energy Balance of Ice Cliffs on Debris-covered Glaciers, Nepal Himalaya. In *Arctic, Antarctic, and Alpine Research* 34 (1), pp. 12–19.

Sakai, A.; Nishimura, K.; Kadota, T.; Takeuchi, N. (2009): Onset of calving at supraglacial lakes on debris-covered glaciers of the Nepal Himalaya. In *J. Glaciol.* 55 (193), pp. 909–917. DOI: 10.3189/002214309790152555.

Schmidli, Jürg (2000): Reconstruction and analysis of mesoscale precipitation in the Alps for the 20th century. With assistance of Christoph Joseph Schär.

SenseFly SA: Parrot Company. Available online at www.sensefly.com, checked on 12/18/2018.

Sensors & Software (2017): www.sensoft.ca, 16/11/2017.

Shepard, Donald (1968): A two-dimensional interpolation function for irregularly-spaced data. In Richard B. Blue, Arthur M. Rosenberg (Eds.): Proceedings of the 1968 23rd ACM national conference on -. the 1968 23rd ACM national conference. Not Known. New York, New York, USA: ACM Press, pp. 517–524.

Shroder, John F.; Bishop, Michael P.; Copland, Luke; Sloan, Valerie F. (2000): Debris-covered glaciers and rock glaciers in the nanga parbat himalaya, pakistan. In *Geografiska Annaler: Series A, Physical Geography* 82 (1), pp. 17–31. DOI: 10.1111/j.0435-3676.2000.00108.x.

Small, R. J.; Clark, M. J. (1974): The Medial Moraines of the Lower Glacier de Tsidjiore Nouve, Valais, Switzerland. In *J. Glaciol.* 13 (68), pp. 255–263. DOI: 10.3189/S0022143000023066.

Swisstopo (2010): Swissimage. Das digitale Farborthophotomosaik der Schweiz. Swisstopo. Available online at https://www.swisstopo.admin.ch/content/swisstopo-internet/de/home/products/images/ortho/swissimage/_jcr_content/contentPar/tabs/items/dokumente/tabPar/downloadlist/downloadItems/588_1464190449870.download/infosi201003deu.pdf, checked on 8/21/2018.

Swisstopo (2018): Hintergrundinformation zur Siegfriedkarte. Edited by Swisstopo. Available online at https://www.swisstopo.admin.ch/de/wissen-fakten/karten-und-mehr/historische-kartenwerke/siegfriedkarte.html, checked on 10/3/2018.

Tanarro, Luis M.; Palacios, David; Andrés, Nuria; Fernández-Fernández, José M.; Zamorano, José J.; Sæmundsson, Þorsteinn; Brynjólfsson, Skafti (2019): Unchanged surface morphology in debris-covered glaciers and rock glaciers in Tröllaskagi peninsula (northern Iceland). In *The Science of the total environment* 648, pp. 218–235. DOI: 10.1016/j.scitotenv.2018.07.460.

Thompson, Sarah; Benn, Douglas I.; Mertes, Jordan; Luckman, Adrian (2016): Stagnation and mass loss on a Himalayan debris-covered glacier: processes, patterns and rates. In *J. Glaciol.* 62 (233), pp. 467–485. DOI: 10.1017/jog.2016.37.

Vere, D. M.; Benn, D. I. (1989): Structure and Debris Characteristics of Medial Moraines in Jotunheimen, Norway: Implications for Moraine Classification. In *J. Glaciol.* 35 (120), pp. 276–280. DOI: 10.3189/S0022143000004615.

Vivian, Robert (1967): Le glacier Noir. In *rga* 55 (4), pp. 733–736. DOI: 10.3406/rga.1967.3352.

Watanabe, O.; Iwata, S.; Fushimi, H. (1986): Topographic Characteristics in the Ablation Area of the Khumbu Glacier, Nepal Himalaya. In *Ann. Glaciol.* 8, pp. 177–180. DOI: 10.3189/S0260305500001415.

995 Watson, C. Scott; Quincey, Duncan J.; Smith, Mark W.; Carrivick, Jonathan L.; Rowan, A. V.N.N.;
996 James, Mike R. (2017): Quantifying ice cliff evolution with multi-temporal point clouds on the debris-
997 covered Khumbu Glacier, Nepal. In *J. Glaciol.* 63 (241), pp. 823–837. DOI: 10.1017/jog.2017.47.

998 World Glacier Monitoring Service (2018): Fluctuations of Glaciers Database. With assistance of
999 WGMS scientific collaboration network of national correspondents and principal investigators as
1000 listed in the related publications above.

1001 Zemp, M.; Huss, M.; Thibert, E.; Eckert, N.; McNabb, R.; Huber, J. et al. (2019): Global glacier mass
1002 changes and their contributions to sea-level rise from 1961 to 2016. In *Nature* 568 (7752), pp. 382–
1003 386. DOI: 10.1038/s41586-019-1071-0.

1004